UNIVERSITY OF CINCINNATI

November 24 19 53

I hereby recommend that the thesis prepared under my supervision by Herbert Katz

entitled The Adsorption Wave in Granular Dessicant Beds

be accepted as fulfilling this part of the requirements for the degree of Doctor of Philosophy

Approved by:

William Licht

Robert W Powell

Nathan Gilbert

Form 668—G.S. and T.C.—1M—4-51

THE ADSORPTION WAVE IN GRANULAR DESSICANT BEDS

A dissertation submitted to the

Graduate School of Arts and Sciences
of the University of Cincinnati

in partial fulfillment of the
requirements for the degree of

DOCTOR OF PHILOSOPHY

1954

by

Herbert Katz

B.Ch.E. City College of New York 1949

M.S. University of Cincinnati 1950

Table of Contents

Table of Contents (continued)

List of Tables

List of Tables (continued)

List of Figures

TABLE OF SYMBOLS

A - cross sectional area of bed container, normal to direction of flow

a - surface area per unit volume of particles

a_p - surface area per particle

B - constant ratio of W to H for linear adsorption isotherm

B' - constant in the Langmuir adsorption isotherm

b - a factor in the kinetic relationship for moisture pickup, proportionality between T and t

C - constant in the Langmuir adsorption isotherm

C' - constant in the equation relating effective surface area to moisture content

c - constant in the equation relating X to Re

D_{Am} - mean diffusivity of water in fluid film

D_I - internal diffusion coefficient

D_p - diameter of a sphere having the same surface area as a given particle

d - constant in the equation relating k_G/G to Re

F - dimensionless ratio $\frac{H - H_i^*}{H_o - H_i^*}$

f - functional notation for relationship between internal diffusion coefficient and average moisture content of particles

G - mass velocity of dry air

H - absolute humidity of air stream

h - length of "dead layer"

I_o - Bessel function of the first kind of zero order and imaginary argument

J - dimensionless ratio $\frac{W - W_i}{W_o^* - W_i}$

K - constant in the equation relating effective surface area to moisture content

K' - constant in the equation relating effective surface area to moisture content

$K_G a$ - overall mass transfer coefficient, based on driving force through the fluid film, expressed as difference in absolute humidity, and a unit volume of particles

k_G - mass transfer coefficient, based on absolute humidities and unit surface area of particles

m - constant in equation relating X to Re

n - constant in equation relating k_G/G to Re

R - radius of particles

Re - Reynolds number

S - a variable of integration

T - a dimensionless parameter, proportional to time, = bt

t - time elapsed from start of run

v - index of summation

W - average moisture content of particles, mass of water per unit mass of dry solids

X - a dimensionless parameter, proportional to distance along the length of the bed

Y - equal to $\sqrt{T} - \sqrt{X}$, using positive roots only

y - equal to $\sqrt{T} - \sqrt{S}$, a variable of integration

z - distance from inlet end to any point in the bed

Z_c - critical bed length

Greek Letters

α - fraction of void volume in the bed

β - fraction of the surface area adsorbing only a single layer of water molecules

φ - functional notation for the probability integral

μ - viscosity of gas stream

ρ_B - bulk density of bed, mass of dry solid per unit volume of container

ρ_G - density of fluid stream

Subscripts

a - refers to actual values of humidity and moisture content, as opposed to values given by the Schumann-Furnas solution

b - refers to conditions at the break time of the bed

f - refers to average values in the fluid film

i - refers to values at zero time

o - refers to values at the bed entrance or at zero moisture content

s - refers to values at the surface of the particle

Superscript

x - refers to values of humidity or moisture content at equilibrium conditions, determined by the adsorption isotherm

ACKNOWLEDGEMENT

The author wishes to express his appreciation to Professor William Licht for his generous assistance in the capacity of thesis supervisor, and to the Research Corporation for its financial assistance in the form of a grant during a portion of this work.

ABSTRACT

Previous contributions to the theory of the adsorption wave in granular dessicant beds have been critically reviewed and several errors pointed out which have not been recognized.

A new theory of unsteady state mass transfer in such cases is presented, based on the assumption that the effective surface area of the particles decreases as the surface becomes covered with water molecules. A theoretical relationship between effective surface area and moisture content is derived from knowledge of the adsorption isotherm. Two new kinetic equations are presented for the cases where mass transfer and internal diffusion, respectively, are the controlling resistances. The kinetic equation for internal diffusion is based on the assumption that the internal diffusion coefficient is a function of the moisture content of the solid. A method is given for determining this function empirically.

Approximate solutions to the differential equations resulting from these new kinetic equations are obtained. A convenient method is given for testing experimental data to determine which, if any, of these kinetic relationships is applicable. A method is outlined for the calculation of quantities which are directly proportional to the mass transfer coefficient k_G and the effective sur-

face area, a, permitting separate correlation of each of these quantities against the Reynolds number.

An experimental procedure was devised and used for testing the new theories presented here. Data are presented for the system air-water-silica gel, showing the effect of varying initial moisture content of the solid, and flow rate of air through the bed. Tests performed on these data show that mass transfer is the rate controlling resistance under the conditions for which this system was studied. These tests also confirm the theoretical relationship between effective area and moisture content.

The experimental results of this investigation can be expressed by the following equation

$$\frac{k_G a}{G} = Re^{-0.31}\left[400 - \frac{188{,}000\ W_i}{1 + 470\ W_i}\right]$$

with an average deviation of ± 9.4 per cent.

Introduction

The operation of separating the components of a mixture of two or more fluids by passing the mixture through a granular solid, which will preferentially adsorb one of the components and allow the others to pass through unchanged, is one which has attracted much attention in recent years.

Whether the fluids are vapors, as in the drying of humid air, or liquids, as in ion exchange or chromatography, the underlying principles of the operation are very similar. This general class of separation processes has come to be known as percolation operations. These operations have found such varied applications as in the decolorizing of crude sugar, the drying of oxygen for high altitude flying, the drying of air for use in various chemical and metallurgical reactions, the separation of hydrocarbons in the petroleum industry, and the removal of toxic gases from the air by a bed of charcoal, as in a gas mask cannister. Although some of these operations have been used for many years, it is only comparatively recently that any extensive theoretical investigations have been undertaken.

Although the results of the present investigation are of general applicability, all subsequent discussions will deal with the application to the drying of humid air, for the sake of simplicity and because the experimental portion of this research was done on such a system.

Consider a fixed bed of a granular dessicant,

through which air of constant inlet humidity is passed at a fixed rate. If the solid is initially moisture free, or nearly so, it will adsorb water vapor from the humid air passing over it. Thus the air leaving the bed will have a humidity very much lower than that of the feed air, and concentration gradients will be set up in the direction of flow in both the fluid stream and the solid. At the beginning of the operation most of the adsorption will occur in a portion of the bed close to the entrance, and so the sharpest concentration gradients will exist in this area. As the dessicant near the bed entrance becomes saturated, the zone in which most of the adsorption occurs, and hence the concentration gradients, begin to move toward the exit of the bed. As soon as these gradients reach the exit of the bed, the humidity of the air leaving begins to rise and, as the latter portion of the bed approaches saturation, becomes equal to that of feed air. It is the movement of these concentration gradients along the length of the bed that is known as the adsorption wave.

The object of any research on this type of operation is to be able to predict theoretically the exact form of the adsorption wave under any given set of conditions. In order to do this some knowledge of the mechanism by which water vapor is transferred from the fluid stream to the interior of the solid is necessary, so as to provide a sound basis for correlating the effects of changes in cer-

tain operating variables. It is the investigation of several of these mechanisms that constitutes the main purpose of this research.

Review of Previous Contributions

There have been in the past three different approaches used to obtain a complete mathematical solution of the adsorption wave. Each of these will be presented in some detail in this section and the assumptions involved in each carefully reviewed.

All mathematical expressions for the adsorption wave represent the solution of a differential equation, which is based on a material balance over the entire bed or some portion of it, and an equation for the instantaneous rate of change of adsorbate concentration of the solid at any point in the bed. In order to write this latter equation, some knowledge of the mechanism by which adsorbate molecules are transferred from the fluid stream to the interior of the solid is necessary. The steps involved in this transfer have been discussed in detail by Klotz (20) and Licht (23) and are as follows.

1. Diffusion, or mass transfer, from the main body of the fluid stream to the surface of the solid particle, through the film surrounding the particle.
2. Physical adsorption, or chemical reaction, at the surface of the solid.
3. Diffusion from the surface to the interior of the solid through the pore structure of the particle.

For the purposes of this thesis it will be assumed that the resistance to step (2) is negligible and so it will not be considered in subsequent discussions. This step has been treated in detail by Klotz (20) and Amundsen (2).

The Schumann-Furnas solution

This treatment was originally presented by Anzelius (2) for the solution of the problem of unsteady state heat transfer from a bed of granular solids to a fluid stream. It was first presented as the solution of the analagous mass transfer problem by Hougen and Marshall (12).

If we consider an element of bed length dz, we may write the following material balance over this element for a period of time dt.

$$GAHdt = GA\left[H + \frac{\partial H}{\partial z}\,dz\right]dt + \rho_B \frac{\partial W}{\partial t}\,Adzdt + \rho_G A\alpha \frac{\partial H}{\partial t}\,dtdz \qquad (1)$$

The first term represents the moisture in the fluid stream entering the section, the second the moisture leaving, the third the moisture picked up by the solid, and the last the change in concentration of water vapor in the fluid trapped in the void spaces of the bed. In writing equation 1 it was assumed that gas density changes due to pressure drop and changes in composition are negligible, diffusion in the fluid stream in the direction of flow are negligible,

and there are no concentration gradients perpendicular to the direction of flow, and no inter-particle diffusion. On simplification equation 1 becomes

$$\frac{\partial H}{\partial z} + \frac{\rho_B}{G}\frac{\partial W}{\partial t} + \frac{a\rho_G}{G}\frac{\partial H}{\partial t} = 0 \qquad (2)$$

In order to solve this equation another relationship between H and W is needed so that one of these quantities may be eliminated. This second relationship is the equation for the rate at which adsorbate is picked up by the solid.

For the rate of mass transfer through the fluid film, Hougen and Marshall (12) have presented the following equation

$$\rho_B \frac{\partial W}{\partial t} = k_G a(H - H_s) \qquad (3)$$

where H_s is the humidity of the fluid stream at the surface of the particle. In order to make any further use of this equation H_s must be related to the average moisture content of the solid. Actually H_s is related to the surface moisture content of the solid by the rate of surface adsorption, and this in turn is related to the average moisture content of the solid by the rate of internal diffusion. Because of the mathematical difficulties involved in attempting to consider all three resistances, it is necessary to assume that one of them is so large compared with the others that it alone controls the overall rate of transfer.

Thus if the resistance to mass transfer is very large, compared with the other resistances, surface adsorption will occur as rapidly as water can be supplied to the surface, which means that H_s is related to W_s by the adsorption isotherm of the system. If also the resistance to internal diffusion is very small, water will diffuse to the interior of the solid as rapidly as it is adsorbed at the surface so there will be virtually no concentration gradient through the solid and W_s will be very nearly equal to W. Thus if mass transfer is the controlling resistance, and if the system exhibits a linear adsorption isotherm, i.e. $W = BH$, equation 3 becomes

$$\rho_B \frac{\partial W}{\partial t} = k_G a \left(H - \frac{W}{B}\right) \tag{4}$$

Upon making the following substitutions in equations 2 and 4,

$$X = \frac{k_G a}{G} z; \quad T = \frac{k_G a}{B\rho_B}\left(t - \frac{a\rho_G}{G} z\right) = b\left(t - \frac{a\rho_G}{G} z\right) \tag{5}$$

differentiating with respect to T, and eliminating W from the resulting equations, the differential equation becomes

$$\frac{\partial^2 H}{\partial X \partial T} + \frac{\partial H}{\partial X} + \frac{\partial H}{\partial T} = 0 \tag{6}$$

In terms of W the differential equation becomes

$$\frac{\partial^2 W}{\partial X \partial T} + \frac{\partial W}{\partial X} + \frac{\partial W}{\partial T} = 0 \tag{7}$$

The case of internal diffusion controlling has been

treated by Wicke (27)(28) and Jury (17). They expressed the rate of internal diffusion in differential form, based on Fick's law of diffusion for a spherical particle. Solving this equation subject to the boundary condition that the surface of the particle was in equilibrium with the constantly changing humidity of the surrounding air, and integrating the result over the radius of the particle, they obtained for the total moisture content at any time

$$W = BH_s - \frac{6B}{\pi^2} \sum_{v=1}^{\infty} \frac{1}{v^2} \int_0^t e^{-\frac{v^2\pi^2 D_I}{R^2}(t - S)} \frac{\partial H_s}{\partial S} dS \qquad (8)$$

where D_I is the internal diffusion coefficient, depending on the size and structure of both the adsorbent and adsorbate, temperature and in some cases on concentration, and S is a variable of integration. In the derivation of equation 8, D_I was assumed to be independent of concentration.

Differentiating equation 8 the rate equation becomes

$$\frac{\partial W}{\partial t} = \frac{6BD_I}{R^2} \sum_{v=1}^{\infty} \int_0^t e^{-\frac{v^2\pi^2 D_I}{R^2}(t - S)} \frac{\partial H_s}{\partial S} dS \qquad (9)$$

Combining this equation with the material balance yields a very complex differential equation which has not been solved. Instead a simplified rate equation was obtained by using only the first term of the series in equations 8 and 9 and com-

bining the two equations to give

$$\frac{\partial W}{\partial t} = \frac{\pi^2 D_I}{R^2} (W_s - W) \qquad (10)$$

If we now assume that the resistance to internal diffusion is very large compared to the other two resistances so that equilibrium exists at the surface and there is virtually no concentration gradient in the fluid film surrounding the particle, equation 10 becomes

$$\frac{\partial W}{\partial t} = \frac{\pi^2 D_I B}{R^2} (H - \frac{W}{B}) \qquad (11)$$

again using a linear isotherm.

Combining equations 2 and 11 and making the following substitutions

$$X = \frac{\pi^2 B D_I \rho_B}{R^2 G} z; \quad T = \frac{\pi^2 D_I}{R^2}(t - \frac{\alpha \rho_G}{G} z) = b(t - \frac{\alpha \rho_G}{G} z) \qquad (12)$$

we again obtain equations 6 and 7. Thus both cases are represented by a single pair of generalized differential equations, differing only in the definition of the dimensionless parameters X and T. For the case where the resistances to mass transfer and internal diffusion are of the same order of magnitude, Jury (15) has shown that since the rates of all three steps must be equal at any time, equations 3 and 10 may be combined to yield the following equation, in terms of the gas film driving force and an overall gas film coefficient, K_G.

$$\rho_B \frac{\partial W}{\partial t} = K_G a \left(H - \frac{W}{B}\right) \tag{13}$$

where

$$\frac{1}{K_G a} = \frac{1}{k_G a} + \frac{R^2}{\rho_B \pi^2 D_I B} \tag{13a}$$

In this case, X and T would be defined by equation 5, using $K_G a$ in place of $k_G a$, and equations 6 and 7 would still apply.

Solutions to equations 6 and 7 have been presented by Hougen and Marshall (12) as follows, subject to the boundary conditions that

$$H = H_o \quad \text{when} \quad X = 0$$

$$W = W_i \quad \text{when} \quad T = 0$$

$$\frac{H - H_i^*}{H_o - H_i^*} = F = 1 - e^{-T} \int_0^X e^{-X} I_o(2\sqrt{XT})\,dX \tag{14}$$

$$\frac{W - W_i}{W_o^* - W_i} = J = e^{-X} \int_0^T e^{-T} I_o(2\sqrt{XT})\,dT \tag{15}$$

Where $I_o(x)$ is a Bessel function of the first order and imaginary argument. It is of interest to note in passing that equations 14 and 15 apply also to the case of a first order reversible reaction controlling, differing only in the definition of the parameters X and T. In addition to the assumptions already mentioned these solutions are based on the assumption that the operation is isothermal.

For gases, the last term in the material balance, equation 2, is generally negligible. It has been shown by Licht (23) that neglecting this term is the same as neglecting the term $\frac{a\rho_G}{G} z$ in the definition of T, equations 5 and 12. If we neglect both these terms, equations 14 and 15 still apply.

These solutions are difficult to use, especially since extensive tables of values of $I_0(x)$ are not available, but they have been presented in graphical form, known as the Schumann-Furnas charts. These charts are in the form of a family of curves giving F and J as a function of T with X as a parameter, and are available in several places in the literature (14) (9). The ranges of F and J generally covered are from 0.01 to 0.9. Since for many applications still lower values are of interest, these charts have been extended by Drew, Spooner and Douglass (7) to include much lower values. By using the series expansion of $I_0(x)$ and performing the indicated integration term by term, they used equation 14 in the following form.

$$F = e^{-X-T} \sum_{v=0}^{\infty} \frac{T^v}{v!}\left(1 + X + \frac{X^2}{2!} + \ldots + \frac{X^v}{v!}\right) \qquad (16)$$

Equation 16 is most useful for low values of X and T. The number of terms required for convergence increases with increasing values of X and T, about ten terms being required for X equal to nine, with T equal to three.

Equations 14 and 16 are both very inconvenient for use in testing experimental data when values of X and b are unknown, since a tedious trial and error procedure must be used. In order to avoid such a procedure Jury (15) has developed a simplified approximate solution as follows. The Bessel function I_o in equation 14 is replaced by the asymptotic expansion

$$I_o(x) = \frac{e^x}{(2\pi X)^{\frac{1}{2}}} \qquad \text{as} \quad x \longrightarrow \infty$$

and it is assumed that $(T/X)^{1/4} = 1$ in the integral which results. Upon simplification this yields

$$F = \tfrac{1}{2}\left[1 + \varphi(Y)\right] \qquad \text{where} \quad \varphi(Y) = \frac{2}{\sqrt{\pi}} \int_0^Y e^{-y^2} dy \qquad (17)$$

$$\text{and} \quad Y = \sqrt{T} - \sqrt{X}$$

Based on this approximate equation Licht (23) has devised a convenient method testing experimental data. From experimental data, generally in the form of a plot of H vs t, a plot of F vs t is constructed. A convenient series of values of F is then chosen and the corresponding values of t read from this plot. Values of $\varphi(Y)$ are then calculated from equation 17 and the corresponding values of Y read from a table of probability functions. For this purpose Licht has prepared a table of values of Y and $\varphi(Y)$ for a series of rounded values of F. If we now plot values of Y vs the corresponding values of $\sqrt{t}$ we should obtain a

straight line of slope $\sqrt{b}$ and ordinate intercept $-\sqrt{X}$. Licht has compared the values of F given by this approximate solution with those given by equation 14. He found excellent agreement for values of X about 20 or greater. If values of X obtained from the plot of Y vs $\sqrt{t}$ are less than this, the data should be checked directly against the Schumann-Furnas charts.

Klinkenberg (19) has found empirically that the accuracy of equation 17 may be improved by changing the upper limit of integration. He suggested the following definition of Y be used in equation 17

$$Y = \sqrt{T} + \frac{1}{8\sqrt{T}} - \sqrt{X} + \frac{1}{8\sqrt{X}} \qquad (18)$$

He presented a nomograph based on this equation, for which he claimed a deviation from equation 14 of $\pm$ 0.006 for X = 2, $\pm$ 0.002 for X = 4 and $\pm$ 0.001 for X = 8, the deviation approaching zero with increasing values of X. While this equation is more accurate than equation 17, it is not as easily adapted to the testing of experimental data.

If experimental data conforms to equation 14, it is theoretically possible to determine which, if any, of the kinetic relationships listed above applies in any given system. This can be done by studying the effect of several operating variables, such as flow rate, particle size and bed length, on the values of X and b. The theoretical dependence of these parameters on various operating

conditions is shown in the table below.

Table I

Effect of Operating Variables on X and b

Variable	Mass Transfer	Internal Diffusion
Flow Rate	$X \alpha d G^{-n}$	$X \alpha 1/G$
	$b \alpha d G^{1-n}$	b - constant
Particle Size	$X \alpha d R^{-1-n}$	$X \alpha \frac{\rho_B}{R^2}$
	$b \alpha d \frac{R^{-1-n}}{\rho_B}$	$b \alpha \frac{1}{R^2}$
Bed Length	$X \alpha z$	$X \alpha z$
	b α constant	b α constant
Temperature	$X \alpha \frac{d(\rho_G D_{Am})_f^{\frac{2}{3}}}{\mu^{\frac{2}{3}-n}}$	$X \alpha B D_I$
	$b \alpha d(\rho_G D_{Am})_f^{\frac{2}{3}}/B\mu^{\frac{2}{3}-n}$	$b \alpha D_I$

Note that the main effect of varying temperature would be in the value of the slope of the adsorption isotherm, which appears in either X or b, but never in both. If both X and b were both found to vary with temperature, it probably means that the resistance to surface reaction is appreciable. If surface reaction were the controlling resistance, b should be independent of flow rate and particle size, and X should vary inversely with flow rate and be independent of particle size.

The effects listed in Table I for the case of mass

transfer controlling are based on the following relationship presented by Gamson, Thodos, Wilke and Hougen (10) (29).

$$\frac{k_G}{G}\left(\frac{\mu}{\rho_G D_{Am}}\right)_f^{\frac{2}{3}} = d\left(\frac{D_p G}{\mu}\right)^{-n} \qquad (19)$$

where d and n are constants to be determined experimentally and the subscript f refers to average values in the film. D_p is taken as the diameter of a sphere having the same surface area as the actual particle used. For example, for a sphere

$$D_p = \sqrt{\frac{a_p}{\pi}}$$

They obtained the following values of d and n, from experimental data on the constant rate drying of regular shaped particles of various solids.

	d	n
$\frac{D_p G}{\mu} > 350$	0.99	+0.41
$\frac{D_p G}{\mu} < 350$	1.82	0.51

Whether the same values of these constants would apply to irregular shaped particles has not yet been determined, although it was assumed in Table I that they do.

It should also be noted that their values of k_G were calculated from experimental values of $k_G a$ by assuming that a is the total geometric surface area of the particles per unit volume of bed. It has been suggested more recently

by Kayser (18) that a is not the true geometric surface area, but is itself a function of the Reynolds number. At very low values of the Reynolds number there are relatively large areas in the bed surrounded by pockets of air which are almost stationary, and hence relatively ineffective for mass transfer. As the Reynolds number is increased the number of such areas decreases and it is only in fully developed turbulent flow that the entire geometric surface area becomes effective. Unfortunately, no method has been developed for the calculation of this quantity, so the correlation of Gamson, et al, must be accepted for the present. A further difficulty involved in the use of the above correlation for irregular shaped particles is the fact that it is extremely difficult to calculate even the true geometric surface area of such particles. Thus the calculation of k_G and the Reynolds number as defined above would be very difficult.

If experimental data conforms with equation 14, but the variation in X and b do not conform exactly to any of the cases listed in Table I, it probably means that more than one resistance is of importance, but the overall resistance remains constant during a run. In this case, the calculated value of X would be proportional to an overall coefficient, and the relative magnitudes of the two resistances may be estimated from equation 13a. By plotting $\frac{1}{K_G a}$ vs $(\frac{1}{D_p G/\mu})^n$, where n is defined on p. 15, we should

obtain a straight line, the ordinate intercept of which would be a measure of the resistance to internal diffusion. It should be recognized, however, that such a procedure is only an approximation, since there is some doubt as to the proper value of n to be used for irregular shaped particles. Varying the value of n to obtain the best straight line would have little significance since it could not be ascertained whether any curvature was due to the use of an incorrect value of n, or to the many approximations made in the derivation of equation 13.

If experimental data does not conform to equation 14 it means that neither of the kinetic relationships presented is applicable. This can mean either that some surface reaction other than a first order reversible is controlling, or that the resistance to mass transfer or internal diffusion, or both, is varying during the course of a run.

Some of the results obtained in testing experimental data against the Schumann-Furnas solution are of particular interest. Licht (23) tested his data and some of Jury's (17), all on the system air-water-drierite, and found that during the early part of a run the data conformed to the Schumann-Furnas solution. After a short time, however, the data began to deviate from this solution, always in such a direction as to indicate that the overall resistance was increasing with time. He attributed this to the fact that as the interior of the solid became filled with

water molecules, the resistance to internal diffusion increased. Thus, while mass transfer was the controlling resistance at the beginning of a run, the resistance to internal diffusion increased sufficiently as the bed approached saturation to cause an appreciable increase in the overall resistance. He also found that values of the mass transfer coefficient apparently increased with increasing bed length. This would seem to indicate that the Schumann-Furnas solution is not applicable to the system in question and in fact defeats the main purpose of such a theoretical treatment, since it prohibits the design of a large scale adsorber from laboratory data. Licht offered as a possible explanation the fact that the dessicant used in Jury's work was not regenerated under uniform conditions. Two runs are cited which are duplicates in every respect except that the dessicant used in one was regenerated for a longer period of time and at a higher temperature. The values of X and b calculated from this run were considerably higher than those from the other one. This variation is in itself unexpected and is difficult to explain on the basis of any existing theory of mass transfer. If internal diffusion were the controlling resistance such behavior might be due to variation of the internal diffusion coefficient with concentration, but Licht has concluded on the basis of the variation of X and b with flow rate that mass transfer is the controlling resistance at

the beginning of a run.

Eagleton (8) also attempted to use the Schumann-Furnas solution to correlate the results of an extensive experimental investigation of three air-water-dessicant systems. The dessicants used were activated alumina, silica gel, and florite. He observed the same manner of variation of resistance with time and bed length, using the Schumann-Furnas solution. His explanation of these variations will be discussed later in this section. It is of interest to note that each of the dessicants used in his work was regenerated at the same time, mixed thoroughly, and allowed to stand at constant temperature a sufficient length of time to eliminate all concentration gradients, prior to use in a test run. It appears therefore, that the explanation offered by Licht for the variation of resistance with bed length is insufficient. Hougen and Marshall (12) used the Schumann-Furnas solution to test the data of Ahlberg (1) on the system air-water-silica gel. They found that the experimentally determined resistances were about 3.57 times the values calculated for mass transfer through the fluid film, using equation 19. This was attributed to the presence of a large additional resistance to internal diffusion. They did not mention any variation of resistance with either time or bed length.

Method of Klotz

Klotz (20) has reviewed an empirical treatment of the adsorption wave originally due to Mecklenburg (24) (25) and extended by several authors. These latter references are classified government documents and hence not available.

Before presenting the details of this method, several new terms must be defined. The break time of bed is arbitrarily defined as the time required for the effluent concentration to reach any specified value known as the break concentration. The life thickness curve is a plot of break time vs. bed length, all other conditions being held constant. The critical bed length is that length of bed whose break time is zero, given by the abscissa intercept of the life thickness curve.

In deriving his relationship, Mecklenburg assumed that up until the break time all of the adsorbate gas in the feed has been picked up by the solid. He also arbitrarily assumed that up until the break time all adsorption has taken place in a portion of the bed near the entrance, and that this portion has become saturated while the remainder of the bed, known as the dead layer, is still completely adsorbate free. Based on these assumptions, he wrote the following material balance

$$GAH_o t_b = W_o^{\times} \rho_B A(Z - h) \qquad (20)$$

where h is the length of the dead layer, and t_b is the break time. If the life thickness curve is linear, the dead layer must be equal to the critical bed length, and equation 20 becomes

$$t_b = \frac{W_o^* \rho_B}{G H_o} (Z - Z_c) \qquad (21)$$

where Z_c is the critical bed length. As pointed out by Klotz, the most serious restriction on this equation is that the life thickness curve must be linear, which not only limits its applicability but requires that a considerable amount of experimental data be available to determine whether or not it is applicable.

In order for equation 21 to be useful, it is necessary to be able to predict the effect of various operating conditions on the critical bed length. It has been shown that the critical bed length is actually the sum of several terms, each representing one of the resistances in the overall transfer. Where mass transfer is the controlling resistance Klotz has presented the following equation for the critical bed length

$$Z_c = \frac{2.303}{a} \left(\frac{D_p G}{}\right)^{0.41} \left(\frac{\mu}{\rho_G D_{Am}}\right)_f^{0.67} \log \frac{H_o}{H_b} \qquad (22)$$

Although no derivation was given for this equation, the author was able to derive this relationship only by starting with equation 14, which at zero time reduces to

$$F = e^{-X} \tag{23}$$

Since the effluent concentration begins to rise at zero time for a bed of the critical length, equation 23 may be written as follows

$$\ln \frac{H_b - H_i^*}{H_o - H_i^*} = -\frac{k_G a Z_c}{G} \tag{24}$$

If H_b is sufficiently small, the effluent concentration will reach that value close to zero time, and the error involved in the use of equation 23 will be small. By neglecting H_i^* and using equation 19 for k_G/G we obtain equation 22. This may then be substituted in equation 21 to obtain a general expression for the break time where mass transfer controls.

If equation 22 was actually derived in the manner just described, there are two questionable points in the derivation which have not previously been pointed out. Equation 14 is based on a rigorous differential material balance, while equation 21 is an approximate material balance based on assumptions previously discussed. It appears that the use of both of them in deriving an equation for the break time is somewhat inconsistent. The second point is that since H_b must be very small in order to use equation 24, this concentration will not differ greatly from H_i^*, and so the error in neglecting H_i^* in this equation may be very great. Apparently most of the

data which has been tested with equation 22 were obtained using freshly prepared adsorbents, so the values of H_1^x were actually zero. Under any other conditions, however, this quantity would certainly have to be taken into account.

The fact that the critical bed length is the sum of several terms is the basis of a method of estimating the relative magnitudes of each of the resistances involved in any particular case. The critical bed length due to mass transfer alone can theoretically be calculated from equation 22 while the actual critical bed length can be determined experimentally from the intercept of the life thickness curve. The difference between these two critical bed lengths is then a measure of the resistances due to surface adsorption and internal diffusion. Theoretical equations for the latter two critical bed lengths may be developed in a manner similar to the derivation of equation 22. This method is actually very similar to the use of an overall coefficient with the Schumann-Furnas solution but requires considerably more experimental data and thus appears to have no distinct advantage. Also this method can only be used for estimation of the break time of a bed, whereas the Schumann-Furnas solution permits calculation of the entire adsorption wave.

It should be noted that for systems which exhibit non-linear adsorption isotherms, this method may be

the only one available for the correlation of experimental data. For most types of non-linear isotherms, a rigorous treatment of the problem leads to very complex non-linear partial differential equations, which have not been solved.

Most of the data which has been subjected to analysis by this method appeared in the classified government documents previously referred to and hence are not available. Klotz, however, has presented the results of tests on two systems. For the system air-chloropicrin-charcoal he presented a plot of critical bed length against flow rate, showing values calculated from equation 22, as well as the experimentally determined values. Since the agreement between the two sets of values was good, it was concluded that mass transfer was the controlling resistance in that system. As a further check on the validity of equation 22, it would be desirable to establish mass transfer as the rate controlling step by some other independent test, but apparently such a test has not been performed. The results of tests on the system air-water-charcoal have also been presented, in the form of a plot of the height of a transfer unit (HTU) against flow rate. The HTU is defined as the critical bed length divided by the logarithm of H_o/H_b. The experimentally determined values of HTU for this system were of the order of several hundred per cent larger than the calculated values, indicating that mass

transfer contributes only a small fraction of the total resistance, the remainder probably being due largely to internal diffusion. It is interesting to note the opinion expressed by Klotz, that in the system air-water-silica gel mass transfer is probably the rate controlling resistance. This is just the opposite of the previously cited conclusions of Hougen and Marshall (12).

Method of Eagleton

Eagleton (8) has presented a method which is similar in many respects to the one just described. Wilson (30) and DeVault (5), in their studies on chromatography, have shown that essentially all the adsorption at any given time occurs over a short length at some location in the bed. This length they called the adsorption band. At first this band is at the bed entrance and then it begins to move downstream toward the effluent end as the initial portion of the bed becomes saturated. During this movement down the length of the bed, the length of the adsorption band may vary. DeVault has shown that when the fluid stream and the solid are in continual equilibrium, the length of the adsorption band as it moves down the bed depends on the shape of the adsorption isotherm. For an

---

After this section was written, some of the material presented here appeared in the following article in the literature: Eagleton, L.C. and Bliss, H. Chem. Eng. Prog. 49 543-49 (1953).

isotherm whose slope decreases with increasing concentration, such as the Langmuir isotherm, the length of the adsorption band decreases as it moves down the bed, the opposite being true for an isotherm curving in the other direction. Non-equilibrium conditions, due to diffusional resistances, cause an increase in the length of the adsorption band as it moves down the bed. Gleuckhauf (26), based on these facts, assumed that when diffusional resistances are present in a system which has an isotherm curving downward, the two opposing effects will balance each other after a short time and the length of the adsorption band will remain constant thereafter. It should be noted that for a system having a linear isotherm, with diffusional resistances present, the length of the adsorption band increases as it moves down the bed, so this method is not applicable to such a system.

Eagleton's treatment of the problem was based on the assumption of constant length of the adsorption band as it moves down the bed. In order to simplify the mathematical treatment he replaced the actual system with an equivalent hypothetical system as follows. In the actual system the adsorption band moves down the length of the bed thus replacing saturated solid at the upstream end with fresh solid at the downstream end, the total length of the band always remaining constant. In his hypothetical system, an adsorption band, of the same length

as the actual one, remains stationary while a continuous supply of fresh solid moves countercurrently to the fluid stream, at a rate equal to the rate of movement of the adsorption band in the actual system. This hypothetical system is illustrated in the diagram below, in which Section I represents the adsorption band. He took material balances around both the sections indicated in the figure

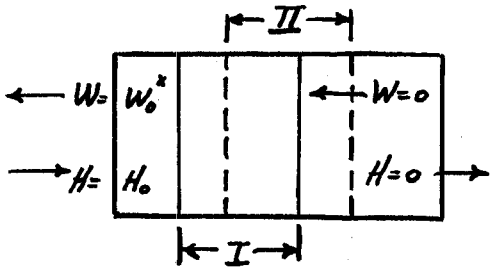

and combined them with a kinetic equation which is a combination of equations 3 and 10. He further assumed that the isotherms for the systems he used could be represented by a straight line but not passing through the origin. Actually he assumed that the isotherm was sufficiently curved to justify the assumption of constant length of the adsorption band, but that it could be represented by a straight line for purposes of calculating driving forces. He then integrated the differential equation based on these assumptions, obtaining two solutions, one for each portion of the isotherm, and an equation to determine the range of applicability of each solution. Based on these solutions he was able to calculate mass transfer coefficients from

data obtained during the initial part of each run, and internal diffusion coefficients from data obtained during the latter portion of a run. Mass transfer coefficients calculated in this manner showed no variation with bed length and gave a fairly good correlation with flow rate. Values of internal diffusion coefficients showed an extremely large amount of scatter, but Eagleton concluded that they showed no variation with either flow rate or bed length.

Eagleton concluded that his results proved the fact that the length of the adsorption band is constant during the course of a run, and attributed the failure of the Schumann-Furnas solution to the fact that it failed to take this into account. This explanation is not acceptable since it was not even necessary to introduce the concept of an "adsorption band" in developing the Schumann-Furnas solution. Actually equation 2 is an exact material balance and completely general, while the material balances he used are at best approximations, so it is difficult to see why his equation should be superior to the Schumann-Furnas solution.

There is one further error in his method which has not been pointed out. Note that the material balance equations are based on the assumption that there is a continuous supply of adsorbate free solid, and that the fluid stream leaving the adsorption band is also adsorbate free.

Obviously these conditions can only be met up until the time the bed breaks. Therefore the use of the resulting equations is meaningless unless they are applied to data obtained very shortly after the bed breaks. In that case this method reduces exactly to that of Klotz, described in the previous section. This also explains the wide variation Eagleton observed in the values of internal diffusion coefficients, since these were calculated from data on the latter portion of each run, when the material balance equations were no longer valid.

New Theoretical Contributions

In view of the inadequacy or limitations of each of the approaches reviewed in the previous section, a careful review of the assumptions involved in each of those equations was undertaken. This review and the new theories which resulted from it are presented in this section.

Comparison of the three solutions presented in the preceding section shows that they are all based on the same kinetic equations, differing only in the material balance equation. Actually equation 2, the material balance used in deriving the Schumann-Furnas solution, is rigorous and completely general, and it is difficult to see how the use of any approximate material balance in its place can be expected to yield a more nearly correct equation. If this is the case, it seems obvious that the failure of the Schumann-Furnas solution must be due to the use of an incorrect kinetic equation. We shall consider the equations for mass transfer and internal diffusion in turn and show why each is incorrect and how it must be modified.

Mass Transfer

Equation 3 for the instantaneous rate of mass transfer is an empirical relationship, apparently based only on analogy with steady state mass transfer, where

such an equation is known to apply. The variables which have been considered in evaluating $k_G a$ in that equation are the same as those considered in steady state mass transfer.

There is, however, a fundamental difference between steady and unsteady state mass transfer which has not previously been considered. Note that the term a is defined as the effective surface area for mass transfer per unit volume of packed bed. In the case of steady state mass transfer, as in heterogenous catalysis, when a molecule is adsorbed on the catalyst surface, it reacts and the reaction products are desorbed, leaving that site available for adsorption of another reactant molecule. In other words, the area available for adsorption is always constant except when we have catalyst poisoning. In that case the presence of strongly adsorbed foreign molecules renders the area they cover ineffective, cutting down the rates of mass transfer and adsorption. In the case of unsteady state mass transfer, such as the drying of air in a fixed dessicant bed, there is a net rate of mass transfer in one direction only. A molecule of water, once adsorbed, either remains on the surface or diffuses toward the interior of the dessicant particle. Obviously, until the particle becomes saturated, the concentration of water molecules on the surface must be greater than or equal to that at any point in the interior

of the particle. Since the average concentration of water is continually increasing, the number of water molecules on the surface must be increasing as the bed approaches saturation. Unless every water molecule on the surface can itself adsorb another molecule and so on to form an infinite number of layers above the surface, that portion of the surface already covered by water molecules is ineffective for further mass transfer. Thus the term a in equation 3 is not constant as previously assumed but decreases with increasing moisture content of the solid. This means that the resistance to mass transfer will be a function of distance along the bed as well as time during the course of a run, and explains the failure of the Schumann-Furnas solution.

Before we can write a new kinetic equation based on this concept of varying area, we must first determine what portion of the total moisture content of the solid has rendered the area it covers ineffective. In order to do this we must consider the physical structure of the solid and the manner in which it holds adsorbate molecules. The surface area of a porous solid is composed of the external surface plus a very large additional surface on the walls of interconnecting pores of varying size running all through the interior of the solid. Movement from the surface of the solid to the interior probably occurs by a combination of diffusion through the gas filling these

pores and a process of hopping from one active site to another further in the interior of the solid. This movement is what we have called internal diffusion and will be considered separately later. In considering mass transfer through the fluid film we are concerned only with the external surface area.

If we have only mono-layer adsorption on the surface, the ineffective area should be directly proportional to the surface moisture content of the solid. Thus, for the total effective area at any time, we would have

$$a = a_o - KW_s \tag{23}$$

where a_o is the total surface area that would be available if the solid were completely moisture free, and K is a constant which is a function of the dimensions of the adsorbate molecule and the manner in which it aligns itself on the surface.

On the other hand, if we had unlimited multi-layer adsorption over the entire external surface, the effective area would remain unchanged, since each molecule on the surface would present an area for further adsorption exactly equal to that part of the area of the original surface which it covered.

For the most general case, the portion of the original area which has become ineffective at any time will be determined not only by the surface moisture content

but also by the number of molecules already on the surface which can support additional layers. This may be determined approximately from consideration of the adsorption isotherm of the system. For a system in which only mono-layer adsorption can occur, the Langmuir isotherm (21)(22) should apply.

$$W = \frac{B'H}{1 + CH} \tag{24}$$

Many systems, however, including the air-water-silica gel system, exhibit what has been called a sigmoid type isotherm. Both these isotherms are represented in the figure below.

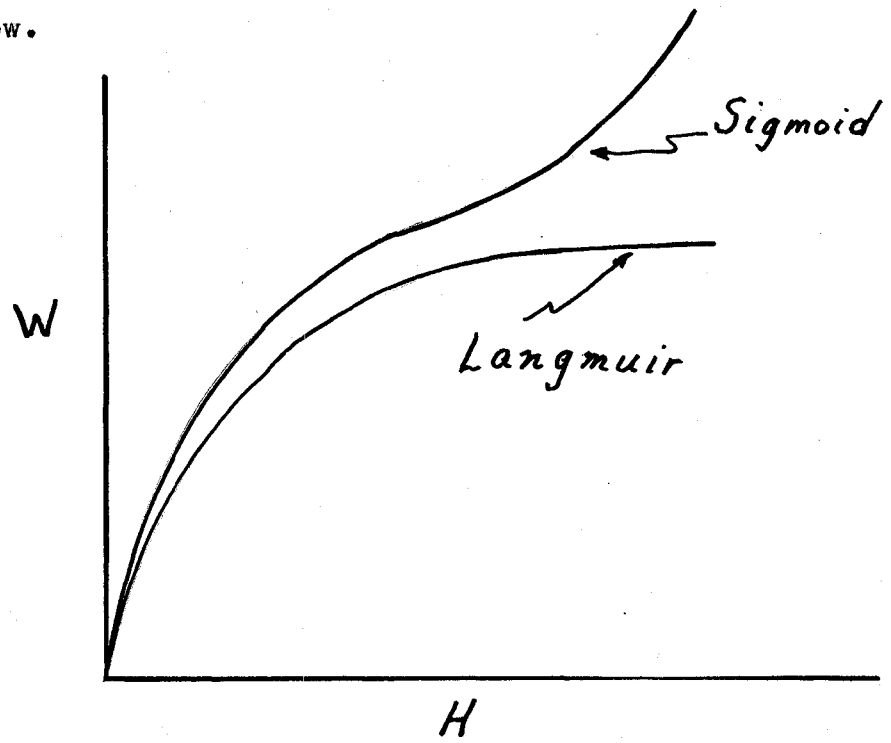

Fig. I - Langmuir and Sigmoid Isotherms

Obviously in a system having a sigmoid isotherm, the equi-

librium moisture content is greater than that predicted by equation 24 for the same humidity, and in fact appears to be increasing indefinitely as the partial pressure of the adsorbate in the gas approaches its vapor pressure. The theory which has had the greatest success in accounting for the sigmoid type isotherm is that of Brunauer, Emmet, and Teller (4). According to this theory, the difference between the Langmuir and sigmoid isotherms is due entirely to multi-layer adsorption. It assumes that as the vapor pressure of the adsorbate gas is approached an infinite number of layers may be built up on a free surface. By a free surface is meant one on which the build up of an infinite number of layers would be unhindered by irregular geometric configurations. The surface of a commercially prepared adsorbent is highly irregular and probably represents a situation where an infinite number of layers may be built up over part of the surface, and a varying finite number over the remaining portion. It is important to note that multi-layer adsorption may occur on some parts of the surface even before there is a single layer over the entire surface.

Based on the above discussion, we will assume that regardless of the actual isotherm of the system, the moisture content in a single surface layer is related to the humidity of the air at the surface by equation 24. The difference between this value and the actual surface

moisture content is due to additional layers on some parts of the surface. A rigorous treatment of the problem from this point on would require knowledge of exactly how many layers each site is capable of supporting. In order to simplify the situation somewhat, we will imagine a surface which can adsorb only a single layer over part of its surface and an infinite number over the rest, the division being made in such a manner that the total surface moisture content of the hypothetical surface will always be the same as that of the actual surface it represents. Call the fraction which can adsorb only a single layer β. We will further assume that the total amount of moisture in a single layer on the surface at any time is distributed over these two areas in a ratio equal to the ratio of the areas themselves. Multiplying equation 24 by β will then give us an expression for the surface moisture content which has rendered the area it covers ineffective. Thus we may write for the effective area at any time

$$a = a_o - \frac{K\beta\ B'H_s}{1 + CH_s} \tag{25}$$

Using this relationship, the new kinetic equation for mass transfer becomes

$$\rho_B \frac{\partial W}{\partial t} = k_G \left(a_o - \frac{K\beta\ B'H_s}{1 + CH_s}\right)\left(H - H_s\right) \tag{26}$$

In order to make further use of this equation,

we must next relate H_s to the average moisture content of the solid. In order to do this we assume equilibrium at the surface and negligible concentration gradient through the solid, as was done in deriving the Schumann-Furnas solution. Although we are dealing with a system exhibiting a sigmoid type isotherm we shall assume that over a small range, for the purpose of evaluating driving forces, we may approximate the isotherm by the linear relationship, $W = BH$. Substituting this in equation 26, with the above assumptions, we obtain after combining constants

$$\rho_B \frac{\partial W}{\partial t} = k_G \left(a_o - \frac{K'W}{1 + C'W}\right)\left(H - \frac{W}{B}\right) \tag{27}$$

With these assumptions, equation 25 becomes

$$a = a_o - \frac{K'W}{1 + C'W} \tag{28}$$

It should be noted here that no assumptions were made in this derivation as to the actual existence of more than a single adsorbed layer. In fact it is probably true that the fraction of the surface covered by more than one layer is extremely small except at high moisture contents, when the interior of the solid approaches saturation. To illustrate the point, consider a molecule adsorbed on the surface of the solid. Another molecule diffusing through the gas film, striking the one already adsorbed, is likely to be held there, even though other

portions of the surface may be bare. If, however, resistance to internal diffusion is very low, the molecule originally at the surface may move toward the interior of the particle almost immediately, still leaving only a single layer on the surface. The important point is that the molecule originally on the surface was capable of adsorbing another molecule. If it had not, the total effective mass transfer area would have been less by the surface area which this molecule covered.

Equation 27 together with the material balance, equation 2 constitute the new set of differential equations. It will be convenient to rearrange equation 27 somewhat before attempting to solve these equations. If we let a_i be the effective area at the beginning of a run we have

$$a_i = a_o - \frac{K'W_i}{1 + C'W_i} \tag{29}$$

Solving for a_o and substituting in equation 27 yields

$$\begin{aligned} \rho_B \frac{\partial W}{\partial t} &= k_G \left[a_i - \left(\frac{K'W}{1 + C'W} - \frac{K'W_i}{1 + C'W_i}\right)\right]\left[H - \frac{W}{B}\right] \\ &= k_G a_i \left[1 - \left(\frac{K'W}{1 + C'W} - \frac{K'W_i}{1 + C'W_i}\right)\right]\left[H - \frac{W}{B}\right] \end{aligned} \tag{30}$$

If we now let

$$X = \frac{k_G a_i z}{G} \quad \text{and} \quad T = \frac{k_G a_i}{B\rho_B} t, \tag{31}$$

neglecting the last term in the material balance, our differential equations become finally

$$\frac{\partial H}{\partial X} + \frac{1}{B}\frac{\partial W}{\partial T} = 0$$

$$\frac{1}{B}\frac{\partial W}{\partial T} = \left[1 - \frac{K'}{a_i}\left(\frac{W}{1 + C'W} - \frac{W_i}{1 + C'W_i}\right)\right]\left[H - \frac{W}{B}\right] \qquad (32)$$

Note that when $T = 0$, $W = W_i$, and these equations reduce to equations 6 and 7.

Internal Diffusion

A complete theoretical treatment of the internal diffusion process would be extremely complex and is considered beyond the scope of this thesis. As previously mentioned, movement of the adsorbate molecule within the solid probably occurs by a combination of more than one mechanism, and these mechanisms have not been clearly defined. Therefore, the use of Ficks law in deriving equation 10 is in itself an approximation. Furthermore, the effect of certain variables on the internal diffusion coefficient is not clearly known. Jury (17) has suggested that this coefficient is a function not only of the external dimensions of the particle but of the pore size distribution within the particle as well. Estimation of this distribution would be extremely difficult, if possible at all. For these reasons, it is probably best to regard D in equation 10 not as a true diffusion coeffi-

cient but merely as a proportionality factor between a rate and driving force, defined by equation 10. In any event, it seems likely, as suggested by Licht (23), that resistance to movement within the solid would increase as the pores became filled with adsorbate molecules. If this is the case, D in equation 10 would not really be a constant, but some function of the moisture content of the solid. We will assume empirically that we can represent this function as follows

$$D_I = D_{I_o} - f(W) \tag{33}$$

where D_{I_o} is the value of the proportionality constant in equation 10 when the solid is completely moisture free and f(W) is some function of the moisture content of the solid, to be determined experimentally.

Substituting this in equation 11 the new kinetic equation becomes

$$\frac{\partial W}{\partial t} = \frac{\pi^2 B}{R^2}\left[D_{I_o} - f(W)\right]\left[H - \frac{W}{B}\right] \tag{34}$$

Defining D_{I_i} as the value of this constant at the beginning of a run we have

$$D_{I_i} = D_{I_o} - f(W_i) \tag{35}$$

Solving for D_{I_o} and substituting in equation 34 we get

$$\frac{\partial W}{\partial t} = \frac{\pi^2 B}{R^2} D_{I_i}\left[1 - \frac{f(W) - f(W_i)}{D_{I_i}}\right]\left[H - \frac{W}{B}\right] \tag{36}$$

If we now let

$$X = \frac{\pi^2 B}{R^2} D_{I_i} \frac{\rho_B z}{G} \quad \text{and} \quad T = \frac{\pi^2 D_{I_i}}{R^2} t,$$

our differential equations become

$$\frac{\partial H}{\partial X} + \frac{1}{B} \frac{\partial W}{\partial T} = 0$$

$$\frac{1}{B} \frac{\partial W}{\partial T} = \left[1 - \frac{f(W) - f(W_i)}{D_{I_i}}\right]\left[H - \frac{W}{B}\right] \tag{37}$$

When $T = 0$, $W = W_i$, and these equations also reduce to equations 6 and 7, assuming internal diffusion to be the rate controlling resistance. Note that these equations are of the same form as equations 32, differing only in the nature of the function $f(W)$.

Solution of Differential Equations

Unfortunately neither of these differential equations, 32 and 37, could be solved rigorously. However, an approximate solution was obtained by a method similar to that used by Douglass (6) on another non-linear partial differential equation. The method will be illustrated with the solution of equations 32, although it is equally adaptable to the solution of equations 37.

We begin by rewriting equations 32 as follows

$$\frac{\partial H_1}{\partial X} + \frac{1}{B} \frac{\partial W_1}{\partial T} = 0$$

$$\frac{1}{B} \frac{\partial W_1}{\partial T} = \left[1 - \frac{K'}{a_i}\left(\frac{W_1}{1 + C'W} - \frac{W_i}{1 + C'W_i}\right)\right]\left[H_1 - \frac{W_1}{B}\right] \tag{38}$$

the subscripts denoting that the quantities H_1, W_1 differ from the values of H and W given by the Schumann-Furnas solution. In integrating this equation, it proved desirable to use two different sets of limits, for reasons which will be discussed on P.83. Using the first set of limits we get

$$\int_{H_1}^{H_o} (\partial H_1)_T = \int_0^X \left[1 - \frac{K'}{a_i}\left(\frac{W_1}{1 + C'W_1} \quad \frac{W_i}{1 + C'W_i}\right)\right]\left[H_1 - \frac{W_1}{B}\right](\partial X)_T$$

or

$$(H_o - H_1)_T = \left[1 + \frac{K}{a_i}\frac{W_i}{1+C'W_i}\right]\int_0^X (H_1 - \frac{W_1}{B})\partial X_T - \frac{K'}{a_i}\int_0^X \frac{W_1}{1+C'W_1}(H_1 - \frac{W_1}{B})\partial X_T \qquad (39)$$

In order to evaluate the integrals on the right hand side of equation 39 we now assume that the values of H_1 and W_1 will not differ greatly from those given by the Schumann-Furnas solution. Therefore the subscripts on the right hand side of equation 39 may be dropped giving as an approximation

$$(H_o - H_1)_T = \left[1 + \frac{K'}{a_i}\frac{W_i}{1+C'W_i}\right]\int_0^X (H - \frac{W}{B})\partial X_T - \frac{K}{a_i}\int_0^X \frac{W}{1+C'W}(H - \frac{W}{B})\partial X_T \qquad (40)$$

From the Schumann-Furnas solution, equations 2, 4 and 5 or 2, 10 and 12, we have

$$-\frac{\partial H}{\partial X} = H - \frac{W}{B} \qquad (41)$$

Integrating this we obtain

$$H_o - H = \int_0^X (H - \frac{W}{B}) \partial X_T \tag{42}$$

Substituting in equation 40 and rearranging we obtain

$$(H_1 - H)_T = - \frac{K'}{a_i} \left[\frac{W_i}{1+C'W_i} (H_o - H)_T - \int_0^X \frac{W}{1+C'W} (H - \frac{W}{B}) \partial X_T \right] \tag{43}$$

In a similar manner we may obtain the following solution for W_1

$$(W_1 - W)_X = \frac{K'}{a_i} \left[\frac{W_i}{1 + C'W_i} (W - W_i)_X - B \int_0^T \frac{W}{1 + C'W} (H - \frac{W}{B}) \partial T_X \right] \tag{44}$$

Integrating equations 38 between the second set of limits we get

$$\begin{aligned} \int_{H_i}^{H_1} (\partial H_1)_T &= \int_X^\infty \left[1 - \frac{K'}{a_i} \left(\frac{W_1}{1 + C'W_1} - \frac{W_i}{1 + C'W_i} \right) \right] \left[H_1 - \frac{W_1}{B} \right] (\partial X)_T \\ \int_{W_1}^{W_o^x} (\partial W_1)_X &= B \int_T^\infty \left[1 - \frac{K'}{a_i} \left(\frac{W_1}{1 + C'W_1} - \frac{W_i}{1 + C'W_i} \right) \right] \left[H_1 - \frac{W_1}{B} \right] (\partial T)_X \end{aligned} \tag{45}$$

Following the same procedure as before we obtain the following set of equations

$$(H_1 - H)_T = \frac{K'}{a_i} \left[\frac{W_i}{1 + C'W_i} (H - H_i)_T - \int_X^\infty \frac{W}{1 + C'W} (H - \frac{W}{B}) (\partial X)_T \right] \tag{46}$$

$$(W_1 - W)_X = - \frac{K'}{a_i} \left[\frac{W_i}{1 + C'W_i} (W_o^x - W)_X - B \int_T^\infty \frac{W}{1 + C'W} (H - \frac{W}{B}) (\partial T)_X \right] \tag{47}$$

The integrals on the right hand side of all these equations may be evaluated graphically, using values of H and W from the Schumann-Furnas charts. For this purpose, it is convenient to rewrite equations 43 and 46 in terms of the quantities read directly from these charts, as follows

$$(F_1 - F)_T = -\frac{K'}{a_i}\left[\frac{W_i}{1 + C'W_i}(1 - F)_T - \int_0^X \frac{W}{1 + C'W}(F - G)(\partial X)_T\right] \qquad (48)$$

$$(F_1 - F)_T = \frac{K'}{a_i}\left[\frac{W_i}{1 + C'W_i} F_T - \int_X^\infty \frac{W}{1 + C'W}(F - G)(\partial X)_T\right] \qquad (49)$$

Equations 44 and 47 may easily be written in a similar manner.

In deciding which equation to use, the following empirical procedure is recommended. For any given value of X there is a value of T for which the two equations will yield the same value of F_1. Determine this value from the intersection of the curves calculated using equations 48 and 49, and for values of T lower than this, use equation 48. For higher values of T, use equation 49.

Note that equations 48 and 49 represent a first approximation of H_1 and W_1. By substituting these values back in equations 43 and 44 and performing the indicated integrations, a second approximation for H_1 may be obtained. A second approximation for W_1 may be calculated

in a similar manner. Successive approximations can thus be made until the calculated value of H_1 is equal to the value used in performing the integrations. While such a procedure should yield an exact solution to equations 38 it would involve so many graphical integrations for the calculation of a single point, that it would generally be impractical.

Testing of Experimental Data

Testing of experimental data against the theories just outlined is based on the fact that at zero time, equations 38 reduce to the Schumann-Furnas solution. At zero time the moisture content of the bed is uniform at W_i and so $k_G a$ is independent of bed length. After a short period of time the moisture content has increased appreciably and there is a considerable concentration gradient along the length of the bed, so $k_G a$ is varying with both time and distance and the Schumann-Furnas solution is no longer valid.

In order to test experimental data, it is therefore necessary to choose a combination of variables such that the bed length is close to the critical, i.e., the exit humidity begins to rise very close to zero time. Under these conditions, if we plot Y vs $\sqrt{t}$ as described on p. 12, we should get a line which is straight for a short time and then begins to curve upward. From the

slope and intercept of the straight portion of this line we may calculate values of X and b, which should then be checked against the Schumann-Furnas charts if necessary. These values should be proportional to the resistance at the constant initial moisture content of the bed, since the moisture content of most of the bed will not be appreciably above this value before the data begins to deviate from the Schumann-Furnas solution. It should be emphasized that such a procedure is not valid for beds whose break time is much greater than zero. A plot of Y vs $\sqrt{t}$ under these conditions will be curving upward by the time a rise in the exit humidity can be measured and any attempt to draw a straight line through these points will yield values of X and b which are too high. This explains the apparent variation of mass transfer coefficient with bed length previously observed.

Thus the procedure for determining the rate controlling resistance will be almost the same as that outlined on p. 14. The only difference in the procedure here is that the initial moisture content will have to be maintained constant throughout such a series of runs, in order to be sure that the observed variations in X and b are due solely to variation in flow rate or particle size. It may also be necessary to vary bed length during the course of such a series of runs in order to have the break time always close to zero.

Using this procedure for the calculation of X and b, we may also verify the assumption that the resistance is a function of moisture content, and determine the exact nature of this function. This can be done by making a series of runs in which all conditions are held constant except the initial moisture content. This is the only way in which we can vary the moisture content in such a manner that it will not vary with bed length, so that the resistance may still be calculated from the Schumann-Furnas solution. The values of X and b calculated from such a set of runs should vary in some regular manner with initial moisture content.

If mass transfer is the rate controlling step we may verify equation 28 as follows. If we multiply equation 28 by $\frac{k_G}{G}$ we get

$$\frac{X}{z} = \frac{X_o}{z} - \frac{k_G K'}{G} \frac{W_i}{1 + C' W_i} \tag{50}$$

On rearrangement this becomes

$$\frac{z W_i}{X_o - X} = \frac{G}{k_G K'} + \frac{G C'}{k_G K'} W_i \tag{51}$$

The value of X_o can be obtained by plotting X vs W_i and extrapolating to zero moisture content. A plot of $\frac{z W_i}{X_o - X}$ vs W_i should then give a straight line of slope $\frac{G C'}{k_G K'}$ and intercept $\frac{G}{k_G K'}$. If the extrapolation to zero

moisture content is doubtful, the data may be fitted directly to equation 50, treated as a three constant equation, by a method such as the method of averages, to obtain values of $\frac{X_o}{z}$, $\frac{k_G K'}{G}$ and C'. Such a fit would provide verification of equation 50 and yield values of the constants for the particular system used. The values of $\frac{K'}{a_i}$, which will be needed later, can be calculated for any value of W_i by dividing $\frac{k_G K'}{G}$ by X/z for the moisture content in question. In this manner it is theoretically possible to calculate values of $k_G K'$ and a_i/K', and correlate each separately against the Reynolds number. This has not previously been possible.

If the internal diffusion is the rate controlling step, we cannot predict the manner in which the resistance will vary with moisture content, but must rectify the resulting curve empirically. The resulting function can then be substituted in equation 37 in order to solve that equation.

In the case where both resistances are important, the procedure would be more complicated. It would be necessary to assume that the values of X are proportional to an overall coefficient, similar to equation 13a. We would then have to make several sets of runs at varying Reynolds numbers, holding the initial moisture content constant dur-

ing each set. From a Wilson type plot, described on p. 16, the resistances to mass transfer and internal diffusion could then be calculated. Each of these resistances could then be correlated against initial moisture content as before, provided that the resistances to mass transfer are calculated at a constant value of the Reynolds number.

All of the tests just outlined can only be made on data obtained at the beginning of a run. In order to determine whether the differential equation is valid during the entire course of a run it will be necessary to utilize equations 48 and 49 in the following manner. Using the values of X and b calculated from the initial portion of a run, the quantities in the brackets on the right hand side of equations 48 and 49 may be calculated for a number of different times, the integrals being evaluated graphically. The corresponding quantities of the left side of these equations may be obtained directly from the experimental data and from the Schumann-Furnas charts. A plot of the quantity within the brackets vs. $F_1 - F$ at a series of different times should be a straight line through the origin of slope $-\frac{K'}{a_i}$. This value of $\frac{K'}{a_i}$ may then be compared with the value calculated from the plot of X/z vs. W_i. A similar test may be made, using the appropriate constants if internal diffusion is the controlling resistance. Unfortunately, the results of such a test cannot

be regarded as positive proof of the validity of the differential equation. If the values of $\frac{K'}{a_i}$ do not check it would be difficult to determine whether this was due to mathematical approximations made in deriving equations 48 and 49, or to an error in the theory upon which the differential equation is based. If, however, the values of $\frac{K}{a_i}$ do check, it is likely that both theory and the approximate solution are correct, since the probability of both being in error by the same amount in opposite directions is small.

In order to test the effect of varying bed length, holding all other conditions constant, we again have to use equations 48 and 49. Since increasing bed length increases the break time, values of X and b cannot be calculated from the Schumann-Furnas solution for longer beds. It is therefore necessary to calculate the adsorption wave for longer beds and compare it with the experimentally determined adsorption wave. Assuming that equations 48 and 49 are correct, this calculation may be performed as follows. From data previously obtained on beds of shorter length, values of X/z and b may be estimated for the known conditions of flow rate, particle size, initial moisture content for the run in question. From this and the known length of the bed, a value of X may be calculated, and values of F_1 at various times estimated from equations 48 and 49. If these calcu-

lated values check the experimental ones, the assumption that X is directly proportional to bed length is verified.

Experimental Work

The purpose of the experimental portion of this work was to test the theory presented in the preceding section and to study the kinetics of adsorption in the air-water-silica gel system. This system was chosen because of the simplicity of obtaining a feed of constant composition and the availability of a continuous method of analysis. Also it exhibits a linear adsorption isotherm over the entire range of humidities used. The isotherm for this system at 80°F is shown in Fig. // in the Appendix.

The experimental procedure consisted essentially of passing feed air of constant humidity at a measured rate through a fixed bed of silica gel of known particle size and measuring the humidity of the effluent stream as a function of time until the bed was nearly saturated.

Experimental Apparatus

The feed air was compressed room air taken from the storage tank of a compressor in which the pressure varied from about 100 to 150 psig. It was passed through two reducing valves in series, the first of which reduced the pressure to about 100 psig and the second ironed out any remaining fluctuations and further reduced the pressure to the desired operating value. The air was then

passed through a long coil of copper tubing immersed in an ice bath, which was contained in a heavily insulated chest. The humidity of the air leaving this dehumidifier could be controlled within limits by varying the pressure of the air in the coils. A trap and blow-off were provided for periodic removal of condensate from the ice chest.

The air leaving the dehumidifier was passed through a needle valve which was used to regulate the flow rate and then through a calibrated rotameter, just prior to entering the test bed assembly. The rotameter was calibrated by the Fischer and Porter Company, the scale reading directly in standard cubic feet per hour of air metered at 70°F and 14.7 psia, with a precision of ± 0.1 cubic feet per hour. For conversion of these readings to mass flow rate, variations in room temperature and barometric pressure were taken into account using the formula given in Fischer and Porter Catalogue Section 98-A.

The test bed assembly consisted of two beds in parallel, with provision for passing air through either bed or both simultaneously. There was also a line to by-pass both beds in order to measure the humidity of the feed air. The beds themselves were merely one-inch brass nipples of various lengths with caps provided with fittings for the attachment of one-quarter-inch copper tubing. The dessicant was supported by wire screens on each end, held in place by small springs in the caps.

The entire assembly was immersed in an insulated metal container which was filled with oil during the regeneration process. Also immersed in this container was a copper coil through which the air passed before entering the bed. This coil served as a preheater for the air blown through the bed during regeneration. The oil bath was provided with an electric heater connected to a temperature controller which was used only during regeneration. An air driven stirrer was also provided to minimize the rather large temperature gradients which would otherwise exist in the bath.

The effluent air from the test bed was then led to the frost point hygrometer, which was used for the measurement of humidity. Jury (16) has presented a detailed description of the design and construction of this instrument. It consisted essentially of a highly polished gold surface on the head of a long hollow copper bolt. This bolt was immersed in an insulated brass tank which was filled with a mixture of dry ice in methanol, which could maintain the surface temperature at about - 90°F. Directly beneath the gold surface on the bolt was a spool wound with a coil of fine nichrome wire, which was connected to a rheostat. Soldered to the underneath side of the gold surface was a fine chromel-alumel thermocouple which was brought out through the bottom of the bolt and connected to a Leeds and Northrup No. 8662 Portable Pre-

cision Potentiometer with a precision of ± 0.001 millivolt. The calibration curve of the thermocouple was taken from Leeds and Northrup Standard Conversion Tables. On top of the gold surface was an optical head which consisted of a small filament lamp, a photo-electric cell and a hollow tube for visual observation of the gold surface.

The light from the lamp was directed on to the gold surface from which a portion of it was reflected to the sensitive element of the photo-electric cell, which was connected to an ammeter. Since the intensity of this reflected light depended on the thickness of the deposit on the surface, the reading of the ammeter was an indication of whether the surface was above or below the frost point of the test air. By varying the setting of the heating coil rheostat, the temperature of the surface was adjusted until a deposit of constant thickness was maintained, as indicated by a constant ammeter reading. At this point equilibrium was assumed to exist between the test air and surface deposit, and the temperature of the surface was determined by means of the thermocouple and potentiometer. The absolute humidity of the test air was obtained from the measured frost or dew point from tables prepared by Licht (23) for this purpose, based on smoothed vapor pressure data from several sources. Between - 40°F and 32°F a deposit of either ice or sub-

cooled water could form, so that in this range it was necessary to observe the deposit visually to determine its nature. The potentiometer readings were recorded to the nearest 0.01 millivolt, corresponding to a precision of ± 0.5°F. The resulting error in the absolute humidity of the test air varied slightly with the temperature and the nature of the deposit, averaging ± 3.0%. Greater precision in surface temperature measurement was not justified because of the error in recording the time of measurement. When the input to the heating coil rheostat was increased, the photo-electric cell current would begin to drop slowly, reach an equilibrium position about which it oscillated for a short time, and finally begin to rise. Because of the lag in the ammeter reading to changes in the thickness of the surface deposit, there was an error of about ± 0.5 minute in measurement of the time at which equilibrium was reached.

Experimental Procedure

The silica gel used in this work was a commercial grade dessicant supplied by the Davison Chemical Company. This material was carefully screened and a sufficient quantity of 10-12 mesh (standard Tyler screen sizes) particles was thoroughly mixed and stored for use during the entire experimental work. The test beds were packed, tamping them at intervals in order to obtain as

nearly a constant bulk density as possible. The test beds were then put in place and regenerated prior to use.

The regeneration procedure was as follows. The air stream was turned on, passing through both beds simultaneously, and a pressure in the dehumidifier of 40 psig and a flow rate of 30 cubic feet per hour was used for two inch beds and this rate was increased proportionally for longer beds. The oil bath was then filled, the controller set at the desired temperature, and the heater and stirrer turned on. After the bath reached temperature, the progress of regeneration was followed with the frost point hygrometer. In order to cool the air from the bath before passing it into the hygrometer, a copper coil was provided at the effluent of the test bed assembly, just outside the oil bath. The process was allowed to continue for one hour after the humidity of the effluent air reached that of the inlet air. At that time the heater and air stream were shut off, and all lines to the beds were closed, except the breather bed which was opened. This was an additional bed outside of the oil bath container, one end of which was connected to the test beds, and the other end remaining open to the atmosphere. The sole purpose of this bed was to prevent humid room air from leaking into the test beds while they were cooling down after regeneration. The oil bath was then drained and the beds allowed to cool. In order to be sure that equilibrium was attained

between the air in the void spaces in the bed and the solid, all beds were allowed to stand at least 12 hours prior to use. In order to check this point, several sets of beds were regenerated and one of each set run after 12 hours, and the other after 24 hours. These beds were run at a very low flow rate so that the value of H_i^* could be measured. It was found that as long as room temperature remained constant any variations in this humidity were within the limits of experimental error. The effect of variations in room temperature will be discussed in detail in the next section.

The procedure for a test run was as follows. The air stream was turned on and directed first through the by pass line. The pressure in the dehumidifier was adjusted to forty psig with a flow rate of 9 cubic feet per hour. After allowing some time for the dehumidifier to reach equilibrium, the hygrometer was prepared for use and the humidity of the feed air measured. The air stream at the same pressure and feed rate was then directed through one of the test beds, the other remaining open to the breather bed. The humidity of the effluent from this bed was measured and it was assumed that this value was the same for both beds. This was checked by measuring H_i^* from several pairs of beds running the two beds in each pair one immediately after the other. In

no case was there a measurable difference in the value of H_i^x.

The flow rate was then adjusted to the desired value, holding the pressure constant at forty psig. Since the temperature of the gold surface depended somewhat on the rate of flow of air across it, the temperature was checked again and the setting of the heater rheostat adjusted if necessary. The breather bed was then closed and the feed stream directed through the second bed, all lines to the first bed being closed. At this point, time measurement was begun. Since the gold surface was at the temperature corresponding to H_i^x and had an equilibrium deposit on it, a rise in the humidity of the effluent from this bed could be detected and measurements begun almost immediately. Since it generally took about ten minutes to build up an equilibrium deposit and adjust the temperature of the surface, this would not have been possible using a single bed. This, plus the fact that the break time of the test beds was too short to allow a reliable measurement of H_i^x, was the reason for using two beds. As soon as the deposit began to build up, the heater current was increased slightly. The deposit would then begin to decrease momentarily, until the rising humidity caught up with the higher surface temperature. When this occured the photo-electric cell current would remain constant for a short time and the surface tempera-

ture and time were read simultaneously. The deposit would then start to build up again and the cycle was repeated. After the surface temperature reached - 40°F it was necessary to clear the surface after each reading, and to look at the deposit each time the temperature was read in order to determine whether the deposit was ice or water. This procedure was continued until the exit humidity reached a value almost equal to that of the feed air.

After disassembling a bed, the contents were heated in a muffle furnace at 500°F for eight hours, and weighed immediately. This, together with measurement of the dimensions of the bed container, was needed for calculation of the bulk density of the bed. This data for each bed is included with the data, in the Appendix, for the last experimental run made on a given bed prior to disassembly.

The apparatus and procedure described here are very similar to those used by Licht (23). More detailed descriptions of some of the apparatus and the technique of using the frost point hygrometer may be found in his thesis.

EXPERIMENTAL RESULTS AND INTERPRETATION

Method of Calculation of X, b, and W_1

As discussed on page 45, calculation of values of X and b were based on the fact that equations 32 reduce to the Schumann-Furnas solution at zero time. The first step in these calculations was to plot Y vs. $\sqrt{t}$, utilizing the approximate Schumann-Furnas solution as described on p. 12. Absolute humidities were obtained from the experimentally measured frost or dew points from the tables prepared by Licht (23) for this purpose. In every case, the plots of Y vs. $\sqrt{t}$ were straight for a short time and then curved upward, as expected. A typical plot is included with the sample calculations in the Appendix on p. 100.

Unfortunately, the values of X calculated from the straight line portion of these plots were all below 20 so that a check against the rigorous solution was necessary. In doing this it was found that the Schumann-Furnas charts, as they are usually presented, could not be used for two reasons. In the first place, the lower limit of F generally given on these charts is 0.01, but for these calculations it was found necessary to begin at about 0.001, since deviations from the Schumann-Furnas solution sometimes became appreciable at values as low as 0.01. Secondly, it is impossible to read these charts

with the degree of accuracy required for these calculations. As a check on the accuracy of these charts, it was noted that if we multiply equation 15 by - 1 and then add 1 to both sides, the right hand side of equations 14 and 15 are of exactly the same form except that X and T are interchanged everywhere they appear. Thus, if we use that chart giving values of F, reading values of X on the T co-ordinate and vice-versa we should obtain from the ordinate, values of 1-G. In a similar manner values of F could be read from either plot. Values of F and G were read in this manner over the entire range of both charts and in most cases gave poor checks. The deviation between the two sets of values varied considerably. Over the range of values of X encountered in this work (up to about 20), the maximum deviation was about 20%. It was therefore necessary to extend the range of these charts and obtain more accurate values. The charts presented by Douglas (6), although extending to much lower values of F, did not include sufficiently low values of X. Additional values were calculated using equation 16, which was found to converge very rapidly for low values of X and T. Points from the charts presented by Douglas as well as the additional point s calculated by the author are tabulated on p. 105 in the Appendix. Comparison of these calculated values with values read from the Schumann-Furnas charts showed that the error in the charts generally is greatest

at very low values of F. The error ranged from zero to as high as 90 per cent in some cases.

From these values, a plot of X vs. T for a number of rounded values of F was prepared. Additional points at T = 0 were calculated from equation 23 and smooth curves drawn through each set of points. In testing an experimental run, values of H/H_0 corresponding to each value of F were calculated and the corresponding times read from the plot of H/H_0 vs. time for that run. Values of X were then assumed, using the value obtained from the approximate solution as a first approximation, and the values of T corresponding to each value of H/H_0 were read from the graph described above. These values of T were then plotted against the corresponding times. This plot should be a straight line through the origin having a slope equal to b as long as the Schumann-Furnas solution holds, and the value of X which gave the best such straight line was accepted as the correct one. Values of b were obtained from the slopes of these lines. Several typical plots are shown in the Appendix on p. 101. The values of X calculated in this manner were always higher than the values obtained from the plot of Y against $\sqrt{t}$. As was expected, the error due to the use of the approximate solution decreased with increasing values of X, the error in X ranging from about 25% at X equal to five, to about 10% at X equal to fifteen.

In calculating the initial moisture content of the beds, the following procedure was adopted. The value of the humidity obtained by running the first bed of each set at a low flow rate was assumed to be the humidity of air in equilibrium with the initial moisture content of the bed. In order to calculate the initial moisture content of the bed from this humidity, it was necessary to know the slope of the adsorption isotherm. As previously mentioned, this initial humidity from beds regenerated under the same conditions showed variation with room temperature. The only explanation that could be found for such behaviour was the variation in the slope of the adsorption isotherm with temperature, which varied over a range of almost 20°F during the course of the experimental work. Although the regeneration process was carried on until equilibrium existed between the feed air and the solid at the regeneration temperature, this equilibrium shifted as the bed cooled down, resulting in transfer of water from the air in the void spaces of the bed to the solid. This transfer continued until a new equilibrium point was reached, and the new equilibrium concentrations depended on how far the bed was cooled down.

Unfortunately, only a small amount of data on the variation of the isotherm with temperature for the air-water-silica gel system could be found. Hougen and Watson (13) presented an equation for the isotherm for

this system, based on data presented by Hougen and Dodge (11). This equation, however, does not represent the data in the region of low concentrations used in the present work. Furthermore, the data of Hougen and Dodge is not in agreement with the more recent data of Eagleton (8), except at extremely low concentrations, while the point calculated by the author is in good agreement with the data of Eagleton. This point represents the moisture content in equilibrium with the inlet humidity used in the present work, and is an average value obtained by graphical integration of the humidity vs. time curves for two runs which were carried to saturation. Because the properties of silica gel may vary somewhat from one batch to another, it was felt that an independent check of the slope of the isotherm would be desirable.

In order to avoid the necessity of making extensive measurements of the adsorption isotherm, the following procedure was devised for obtaining the slope of the isotherm directly from experimental measurement of the adsorption wave. From the definitions of X and b, regardless of which kinetic equation applies, note that

$$\frac{X}{b} = \frac{z_B \rho_B}{G}$$

Using this equation, values of B were calculated from the calculated values of X and b, and the measured values of bed length, flow rate, and bulk density for each run.

These calculated values of B are shown in Fig. 2, plotted on a logarithmic scale against the reciprocal of the absolute temperature. Although there is considerable scatter, the trend is evident. In addition to the cumulative experimental errors which affect the values of B, there is an error in the values of room temperature. The error in these readings is $\pm$ 0.5°F, and the entire range of temperatures covered was 18.5°F. The line in Fig. 2 was drawn by eye. There is no reason why this type of plot would have to be a straight line, and a better fit of the data might be obtained with a curve. However, since this data was not used in subsequent calculations, except in the calculation of the adsorption wave for Run 23, neither more precise temperature measurement nor a more elaborate curve fitting procedure was necessary. At 80°F, the slope of the isotherm read from Fig. 2 is 59.0, which is in fair agreement with the value of 48.2, read from the slope of the line in Fig. 11 . Over the range of initial moisture contents covered in this work, there is a 2.7 fold increase in the slope of the isotherm from 90°F to 70°F, according to the data of Hougen and Dodge. The increase over this temperature range on Fig. 2 is 3.1 fold.

From the values of B calculated in this manner, and the measured value of H_1^*, the initial moisture content of the bed was calculated.

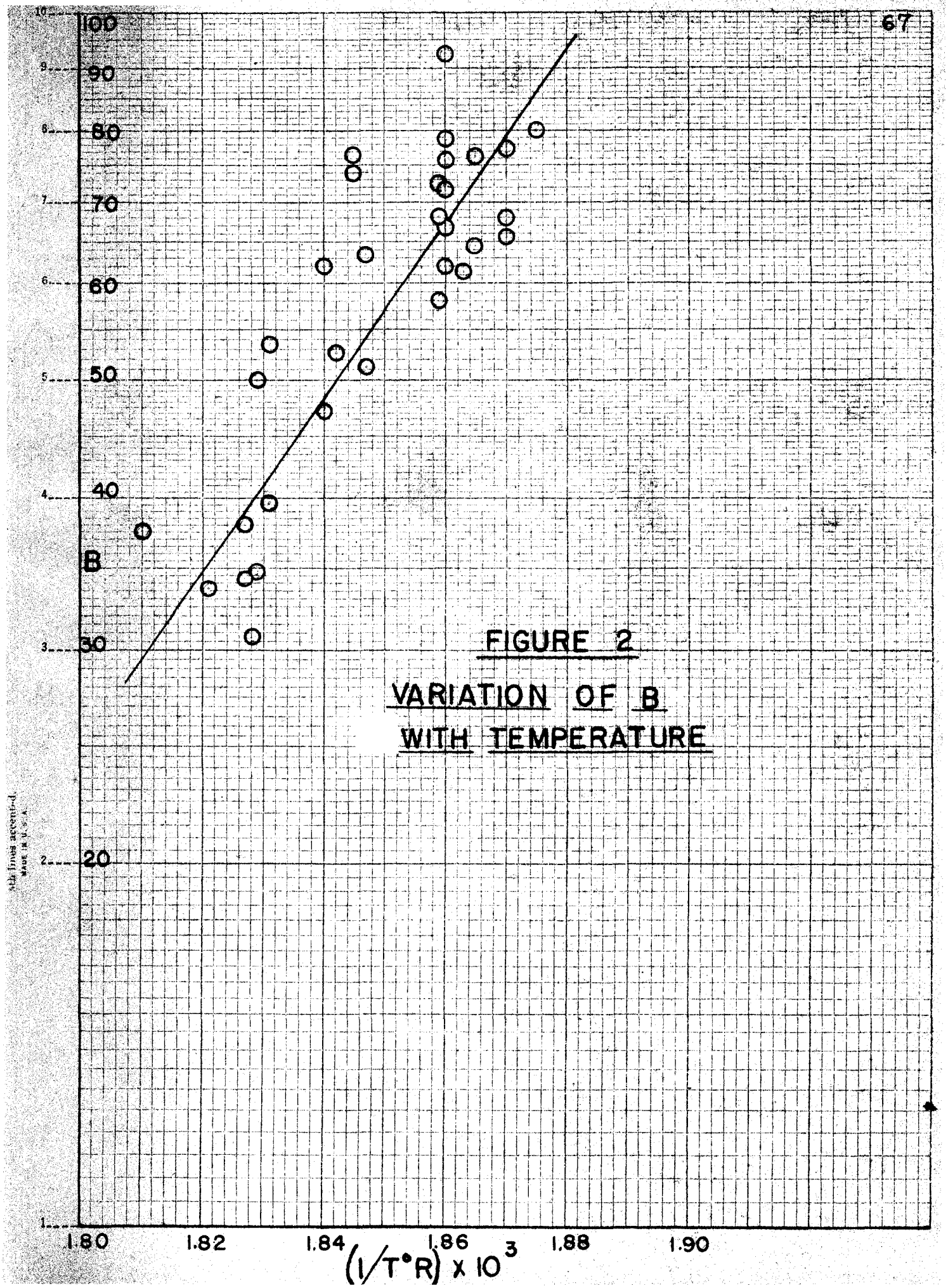

FIGURE 2

VARIATION OF B WITH TEMPERATURE

Effect of Initial Moisture Content

The purpose of the first set of experimental runs was to test the theory previously presented as described on p. 47 . The original data for all these runs may be found in Tables in the Appendix. Plots of several typical runs are shown in Fig. 3. The results of this series of runs are shown in Fig. 4, which is a plot of X/z vs. W_i. A plot of b vs. W_i was also constructed, but it showed somewhat greater scatter than Fig. 4. Because of the variation of the slope of the adsorption isotherm with room temperature, it was desirable to plot that parameter which is independent of B. From equations 5 and 12, it is obvious that this depends upon which resistance is controlling. The fact that the plot of b vs. W_i showed greater scatter was attributed to the fact that mass transfer is controlling for this system. Since the results of additional tests confirmed this fact, only the plot of X/z vs. W_i is presented here. Eighteen of the runs in this set were made on two different two inch beds, holding everything constant except the conditions of regeneration, and the bulk density, which varied only slightly from one bed to another. In adjusting the flow rate during this entire set of runs, room temperature and barometric pressure were taken into account and the setting of the rotameter varied accordingly so as to main-

FIGURE 3
EFFECT OF INTIAL MOISTURE CONTENT ON BED PERFORMANCE

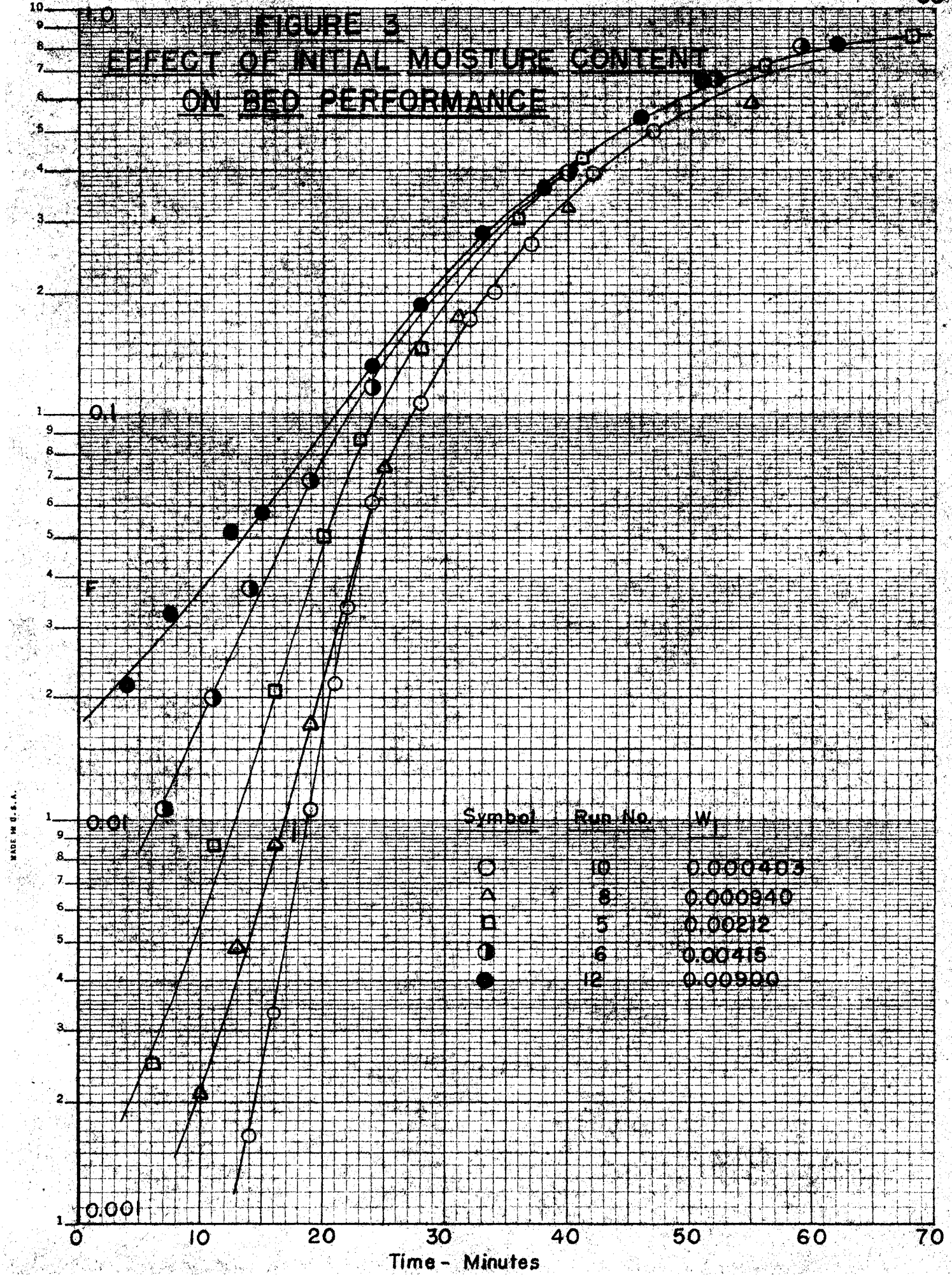

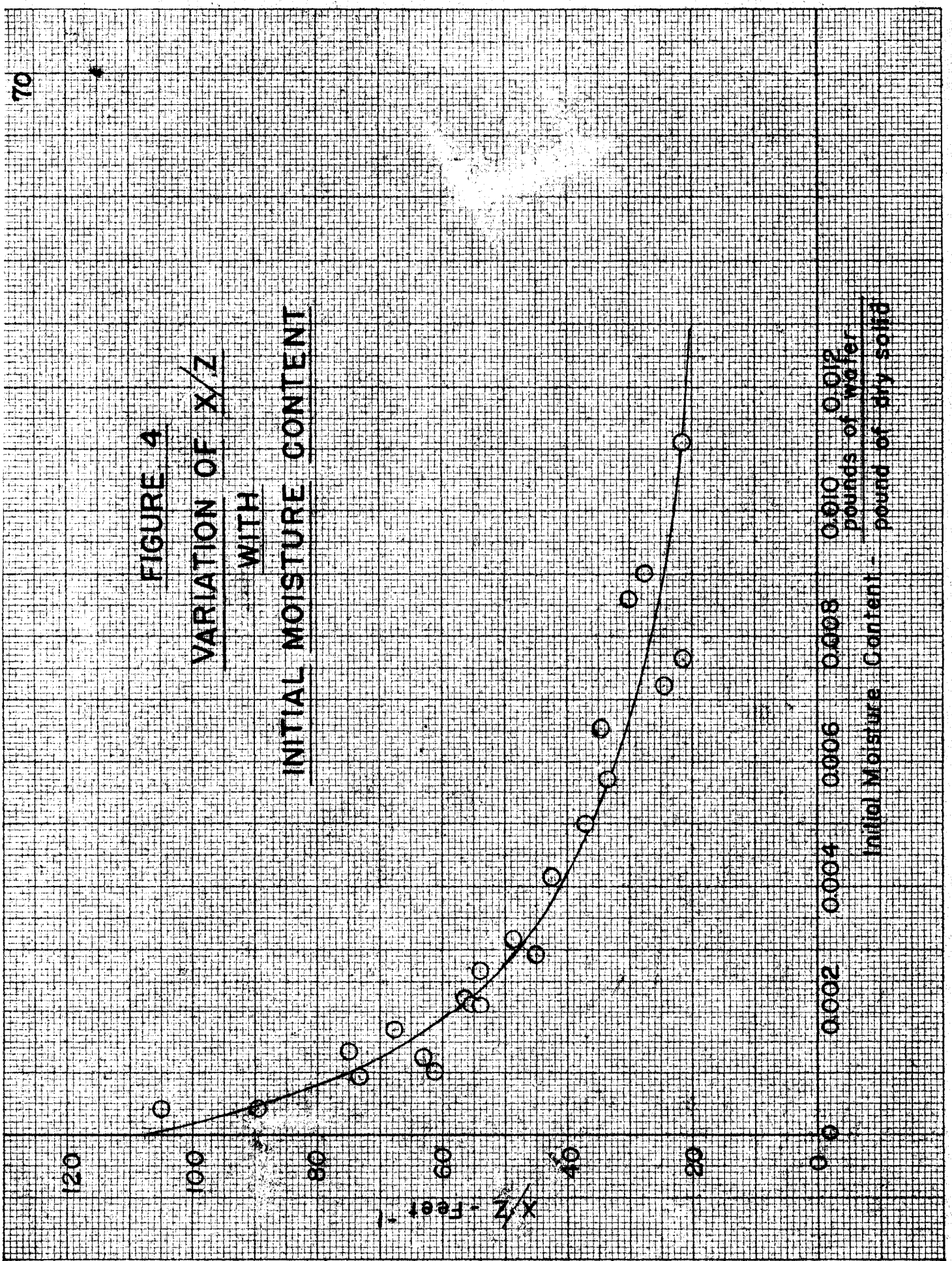

FIGURE 4

VARIATION OF X/Z WITH INITIAL MOISTURE CONTENT

tain a constant mass flow rate. The regeneration temperature used varied from 140 to 230°F. In order to be sure that the observed variation in the values of X was not due to some purely mechanical effect caused by varying the regeneration temperature rather than to variation in moisture content, five of these eighteen runs were made on beds regenerated at 170°F. Variation in initial moisture content for these runs was produced by varying the pressure in the dehumidifier during regeneration from 10 to 80 pounds per square inch gage. Since the points on Fig. 4 representing these runs show no consistent deviation from the curve defined by the rest of the points the shape of the curve appears to be due solely to the variation in initial moisture content. Further evidence in support of this statement is the fact that the order of varying regeneration temperatures for the runs made on any one bed was purely random. It does not seem likely that any effect other than varying initial moisture content would be reversible, so if such effects were present we would not expect a smooth variation in values of X, unless runs were made in the order of increasing regeneration temperature.

The conditions of flow rate, particle size and bed length chosen for this set of runs was such that, at the highest initial moisture content used, a two-inch bed was considerably shorter than the critical bed length.

This meant that as soon as a test run on these beds was begun, there was a sudden sharp increase in the exit humidity and it took some time before the temperature of the gold surface could be readjusted and accurate humidity readings obtained. In order to improve the accuracy of the data in the region of high initial moisture content, it was therefore necessary to make several runs on longer beds. The results of three such runs, made on beds three, four, and five inches long, are also included in Fig. 6. In addition, one run made on a three inch bed regenerated at 170°F is included. It is significant that these points lie along the same curve drawn through points representing runs made on two inch beds. This is some indication that values of X calculated in the manner described from the initial portion of a run do not show variation with bed length, as was previously observed with the Schumann-Furnas solution.

The curve drawn in Fig. 4 was calculated from equation 50 using the following values of the constants:

$$X_o = 107.6 \frac{k_G K'}{G} = 47900 \text{ ft.}^{-1} \quad C' = 469 \frac{\text{lbs. dry solid}}{\text{lb. water}}$$

These constants were obtained by fitting all the points shown on Fig. 4 to equation 50 using the method of averages. The average deviation of the points on Fig. 4 is ± 7.0%. In attempting to rectify equation 50 it was found that a considerable range of values of X_o could be

obtained by extrapolation of the data in Fig. 4. Therefore the method of averages was used, treating equation 50 as a three constant equation.

In addition to the experimental errors previously discussed there is another factor which may account for some of the scatter in Fig. 4. If the resistance to mass transfer accounts for an appreciable portion of the total resistance, all the runs in Fig. 4 should have been made at a constant Reynolds's number. Even though adjustments were made to keep G constant, there was a maximum variation of about 4 per cent in the Reynold's number due to the variation of the viscosity of air with room temperature. Also the variation in bulk density of the beds caused some variation in the mass transfer coefficient.

The main conclusion that can be drawn from the results shown in Fig. 4 is that the overall resistance to transfer is a function of the moisture content of the solid, confirming the main assumption upon which equations 48 and 49 are based. Furthermore, the variation in resistance with moisture content may be expressed by equation 50, within the limits given above. We cannot, however, accept this as confirmation of the other assumptions upon which equation 50 is based. The values of X in Fig. 4 may represent the resistance to internal diffusion or some combination of mass transfer and internal diffusion.

Effect of Varying Reynold's Number

The second set of runs was designed to determine the relative magnitudes of the various resistances involved in the air-water-silica gel system. The results of this set of runs are shown in Fig. 6, in which X/z is plotted against the Reynold's number. The original data for these runs may be found in Tables in the Appendix. Plots of several typical runs are shown in Fig. 5. These runs were all made on 10-12 mesh silica gel, at flow rates varying from 272 to 1161 pounds per hour per square foot.

Since the calculation of values of X depended on the fact that the break time of the bed was close to zero, it was necessary to vary bed length along with flow rate in order to meet that condition. Therefore, the results shown on Fig. 6 include runs made on two, three, and four inch beds. The fact that all these points fall on a single straight line is further evidence that overall mass transfer coefficients calculated in this manner are independent of bed length.

As previously mentioned, in studying the effect of varying Reynold's number, the initial moisture content of all beds should be the same. For this set of runs, a regeneration temperature of 170°F was arbitrarily adopted. This gave initial moisture contents which permitted accurate, rapid measurement of H_1^x and still allowed a sufficiently wide range of exit humidities to work over.

Even though the conditions of regeneration were held constant, there was some variation in initial moisture content during this set of runs due to variation in room temperature, which accounts for some of the scatter in Fig. 6. Variation in room temperature might have an additional effect if more than one resistance were important. In this case the values of X_o/z in Fig. 6 would be proportional to an overall mass transfer coefficient, which would be dependent to some extent on the slope of the adsorption isotherm. This might also account for some of the scatter in Fig. 6.

In calculating Reynold's numbers, the average of the mesh openings of 10 and 12 mesh Tyler screen sizes was used for the diameter. Since Gamson et al (10)(29) used the square root of the surface area per particle, the numerical values of Reynold's numbers on Fig. 6 cannot be compared with their values. It would be extremely difficult to measure the surface area of the irregular particles used in this work, and there is no real reason to believe that this dimension would have any greater significance for irregular shapes than the one used.

Theoretically, it is possible to correlate the results of both Fig. 4 and 5 by the use of a single equation, by use of equation 50 in the following form,

$$\frac{X}{z} = C\,Re^{n} - d\,Re^{m}\,\frac{W_i}{1 + C'W_i} \qquad (52)$$

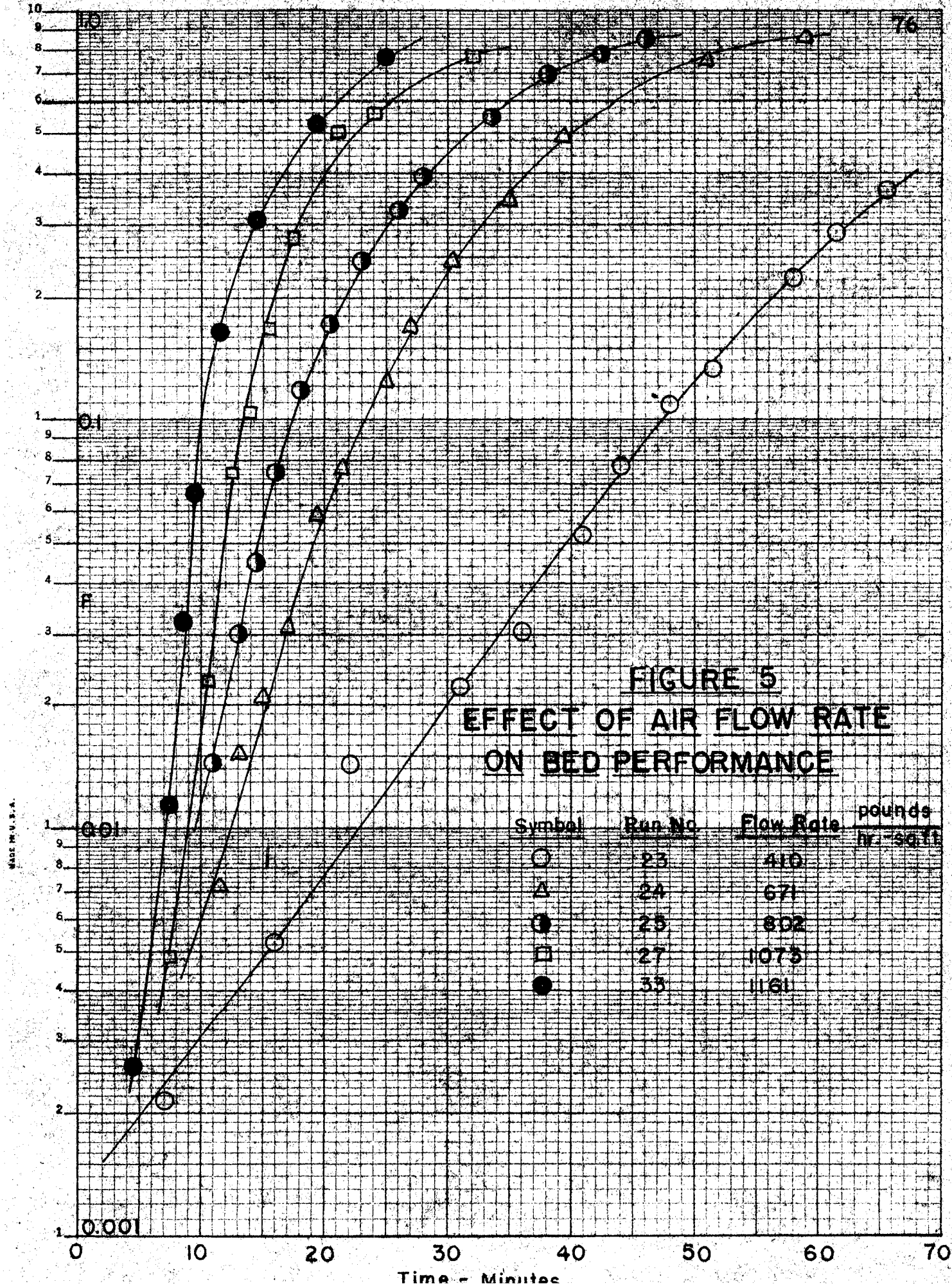

FIGURE 5

EFFECT OF AIR FLOW RATE ON BED PERFORMANCE

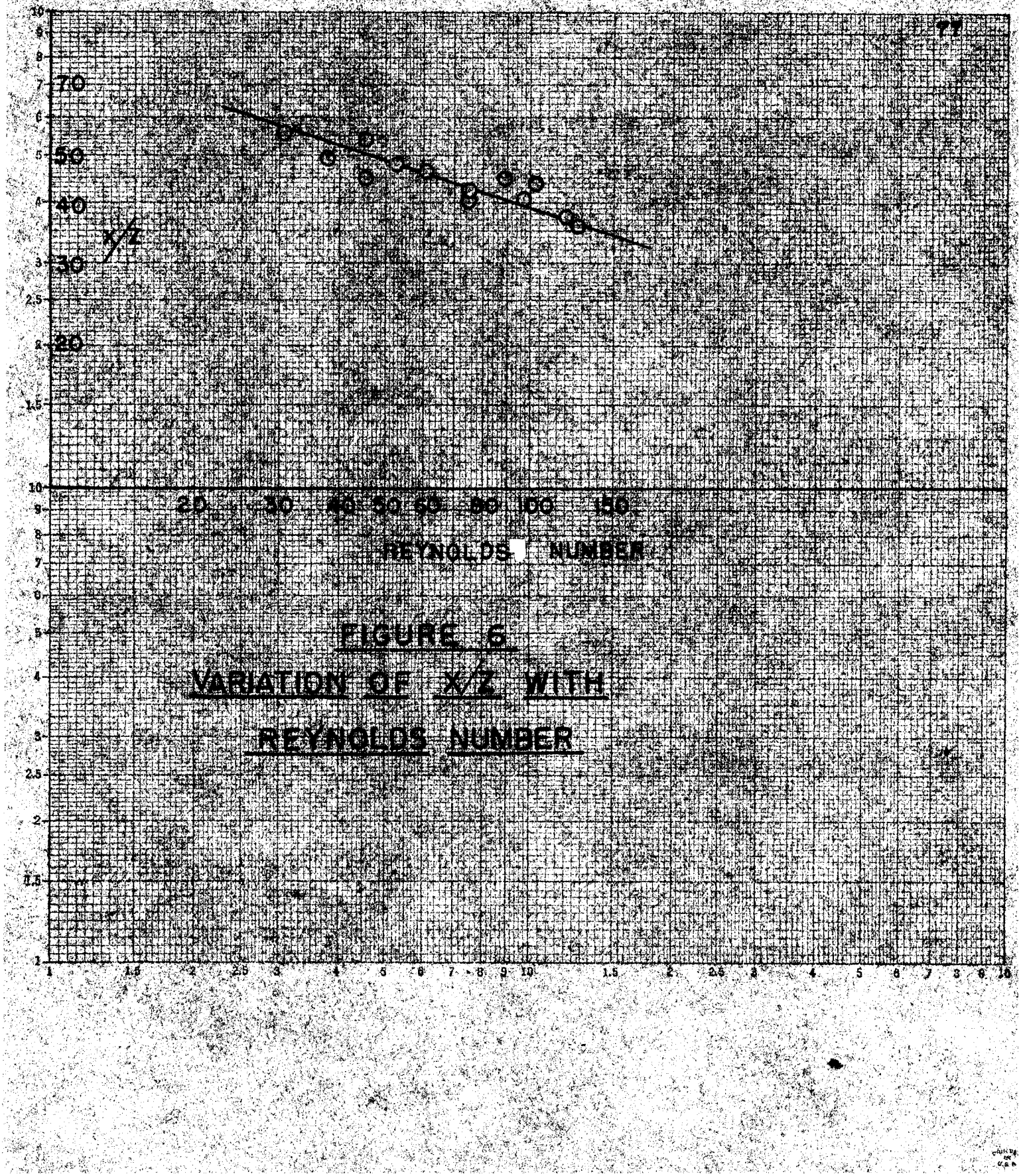

FIGURE 6

VARIATION OF X/Z WITH

REYNOLDS NUMBER

where

$$\frac{X_o}{z} = \frac{k_G a_o}{G} = C\ Re^n \quad \text{and} \quad \frac{k_G K'}{G} = d\ Re^m$$

If internal diffusion were controlling equation 52 would apply if we let

$$\frac{X_o}{z} = \frac{\pi^2 B \rho_B D_I}{R^2 G} = c\ Re^n$$

and

$$\frac{\pi^2 B \rho_B K'}{R^2 G} = d\ Re^m$$

In order to utilize this equation for mass transfer controlling it would be necessary to correlate values of X_o/z and $k_G K'/G$ separately against the Reynolds number. This was attempted by utilizing equations 48 and 49 for the calculation of K'/a_i for each run. With this quantity and the known values of X and W_i, X_o and $k_G K'/G$ could be calculated. Unfortunately, reliable values of K'/a_i could not be calculated in this manner. In lieu of a more exact solution to the differential equation, the most reliable method of obtaining such a correlation would be to make a series of runs similar to that shown in Fig. 4, at a number of different flow rates. Values of X_o/z and $k_G K'/G$ could then be calculated in the manner already described and separately correlated against flow rate. Such a procedure, while undoubtedly reliable, would require a very large amount of experimental data for each system.

Since neither of the above methods could be used with the data available, an attempt was made to fit the data shown in Fig. 6 to equation 52, evaluating the constants by a trial and error procedure. However with four constants and only thirteen experimental points, it was found that the data could be represented using a considerable range of values of m and n, if the values of c and d were adjusted appropriately. It was then noted that, according to equation 52, a logarithmic plot of X/z vs. Reynolds number should not be a straight line if mass transfer is controlling unless m is equal to n, and W_i is constant. In view of the fact that the data on Fig. 6 do fall very nearly on a straight line, it was considered a reasonable simplification to assume that m is equal to n. As can be seen from equation 52, this is equivalent to assuming that the effective surface area is independent of the Reynolds number. Although we cannot tell definitely from the present data whether or not this is actually the case, the resulting equation fits the data fairly well. If internal diffusion were controlling, obviously m = n = -1.

The constants in equation 52, with m equal to n, were then evaluated by the method of averages. The resulting equation is

$$\frac{X}{z} = Re^{-0.31}\left[399 - 188{,}000\,\frac{W_i}{1 + 469W_i}\right] \qquad (53)$$

This equation represents the data with an average deviation of ± 9.4 per cent. The line on Fig. 6 is the best straight line drawn through a series of points calculated from equation 53, using the experimentally measured flow rates and initial moisture contents.

According to Table 1, if internal diffusion were the rate controlling resistance the exponent in this equation should be -1. If mass transfer were controlling and the work of Gamson et al were applicable, the exponent should be either - 0.41 or - 0.51 depending on the range of Reynold's numbers. If we had a combination of both resistances, the exponent would probably be somewhere in between these two extremes. Obviously internal diffusion is not the rate controlling resistance. It appears that at least the major portion of the total resistance is due to mass transfer. The exponent of - 0.31 does not compare favorably with those reported by Gamson et al. This could be due to the fact that mass transfer coefficients for irregular shaped particles show greater variation with Reynolds number than in the case of regular shaped particles. However, since a considerable range of values of m and n in equation 52 represented the data equally well, no special significance can be attached to the exponent - 0.31. For purposes of comparison with values reported for regular shaped particles it would be necessary to correlate X_o and $k_G K'/G$ separately against the Reynolds number, in the manner

described on p. 78 .

One further test was attempted with this data in an effort to confirm the conclusions just drawn. This was the use of a Wilson type plot as discussed on p. 16 . Such a plot is shown in Fig. 7 on which $1/K_G a$ is plotted against $1/G^{0.59}$ and against $1/G^{0.49}$. It was necessary to use two different exponents since the range of Reynold's numbers obtained could not be compared with the ranges in which Gamson et al recommend the use of each of the exponents used.

With an exponent of 0.59, the extrapolated curve would very nearly pass through the origin. With an exponent of 0.49, the curve would give a negative intercept, which would be meaningless. In any event, it does not seem possible that either of the curves in Fig. 7, would show a large positive ordinate intercept. Therefore, assuming that the results, obtained by Gamson et al are applicable to irregular shaped particles, we may conclude that the resistance to internal diffusion is negligible. This fact, combined with the results shown in Fig. 4, confirms the assumptions upon which equation 50 is based.

Test of Approximate Solution

In order to test the validity of equations 48 and 49, several of the runs represented in Fig. 4 were

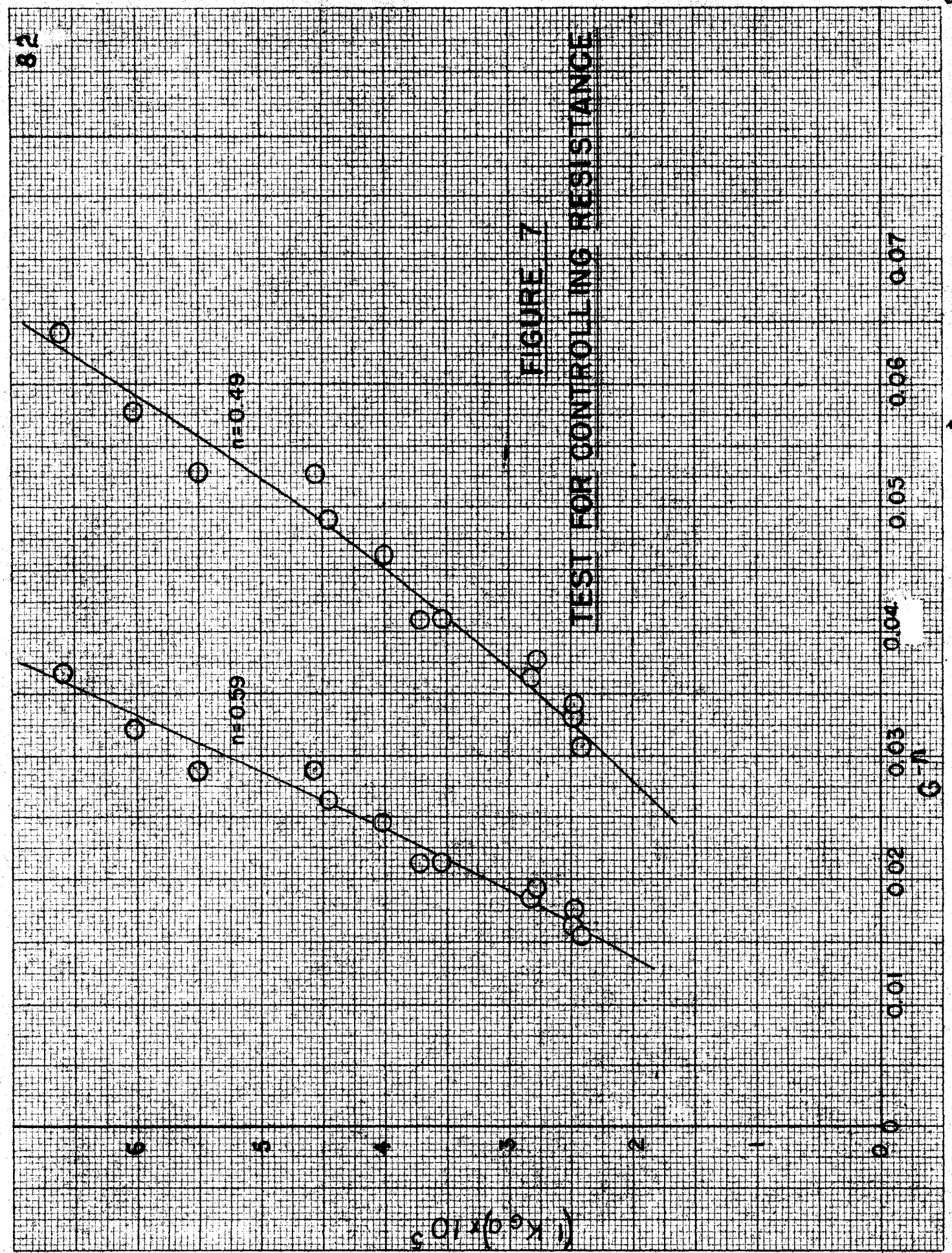

82

tested by the method described on p.49 . At first only equation 48 was used for this, and it was found that the resulting plot of $F_1 - F$ vs. the quantity within the brackets was not a straight line, as had been expected. The slope of the resulting curves approached the value of K'/a_i calculated from Fig. 4 at high values of F, but the error was very large at low values of F.

Careful study of equation 48 showed that at least part of the error was due to the fact that it does not satisfy the boundary condition that $F = 0$ at $X = \infty$. In order to meet this condition, the integral in equation 48, taken from zero to infinity must equal $W_i/1 + C'W_i$. Actually, because F and G were used in evaluating this integral instead of F_1 and G_1, the value of the integral was always too large. It was for this reason that equation 32 was integrated between two different sets of limits. Equation 49, while satisfying the boundary condition at X equal to infinity, does not satisfy the boundary condition that $F_1 = 1$ at $X = 0$. It was found that the use of both equations 48 and 49, each in a region far removed from the boundary condition it does not satisfy gave better results than the use of either equation alone. The use of equation 49 is recommended starting at F equal to zero, until the two solutions intersect. For values of F higher than that corresponding to the point of intersection, equation 48 gives better results. In using equation 49 the

quantity within the brackets was always negative, yielding negative values of $F_1 - F$. The reason for this is not apparent, but the absolute values of this quantity was used in all calculations, with good results. In integrating from H_1 to H_0, the humidity is decreasing from X equal to zero to any given value, and since the actual resistance is higher than was used in deriving the Schumann-Furnas solution, the rate of decrease will be less and we would expect the actual humidity to be higher. In integrating from H_i^x to H_1 the humidity is increasing from X equal to infinity to any given value, but the rate of increase is less than that given by the Schumann-Furnas solution, so we would expect the actual humidity to be less. If, in the latter case, we measure distance from infinity to zero rather than in the other direction, the sign of $\frac{\partial H}{\partial X}$ would change, and equation 49 would then yield positive values of $F_1 - F$.

While the use of both these equations gave better results, it was found that reliable values of K'/a_i still could not be calculated in this manner. These equations are, however, useful for design purposes. Note that an error as large as one hundred per cent in the calculated value of $F_1 - F$ can still give results closer to the experimental values than the Schumann-Furnas solution, but for purposes of correlating K'/a_i against the Reynolds number, an error of this magnitude could not be tolerated.

Using values of K'/a_i calculated from the results of Fig. 4, the adsorption waves for three typical runs were calculated in this manner and are shown in Fig. 8, 9, and 10. Also shown on these figures are curves calculated from the Schumann-Furnas solution. As was expected, these latter curves in every case lie below the experimental curves. The points calculated from equations 48 and 49 are, in almost every case, closer to the experimental values than those calculated from the Schumann-Furnas solution. It is, however, difficult to tell from these results whether or not the differential equations presented here are valid during the entire course of a run.

These equations were also tested on several runs made at varying flow rates. For these calculations, values of K'/a_i were also obtained from Fig. 4, assuming that this quantity is independent of flow rate. The results of these calculations are shown in Fig. 8 and 9. It appears that equations 48 and 49 do not work as well in this case. This may be due in part to the use of incorrect values of K'/a_i. Apparently K'/a_i is a function of flow rate, but, as discussed on p.16 the exact nature of this variation could not be determined from the data available.

One further attempt was made to determine whether or not the theory upon which equations 48 and 49 are based accounts for the behaviour of a bed during its entire life. By graphical integration of a plot of $H_o - H$ against time,

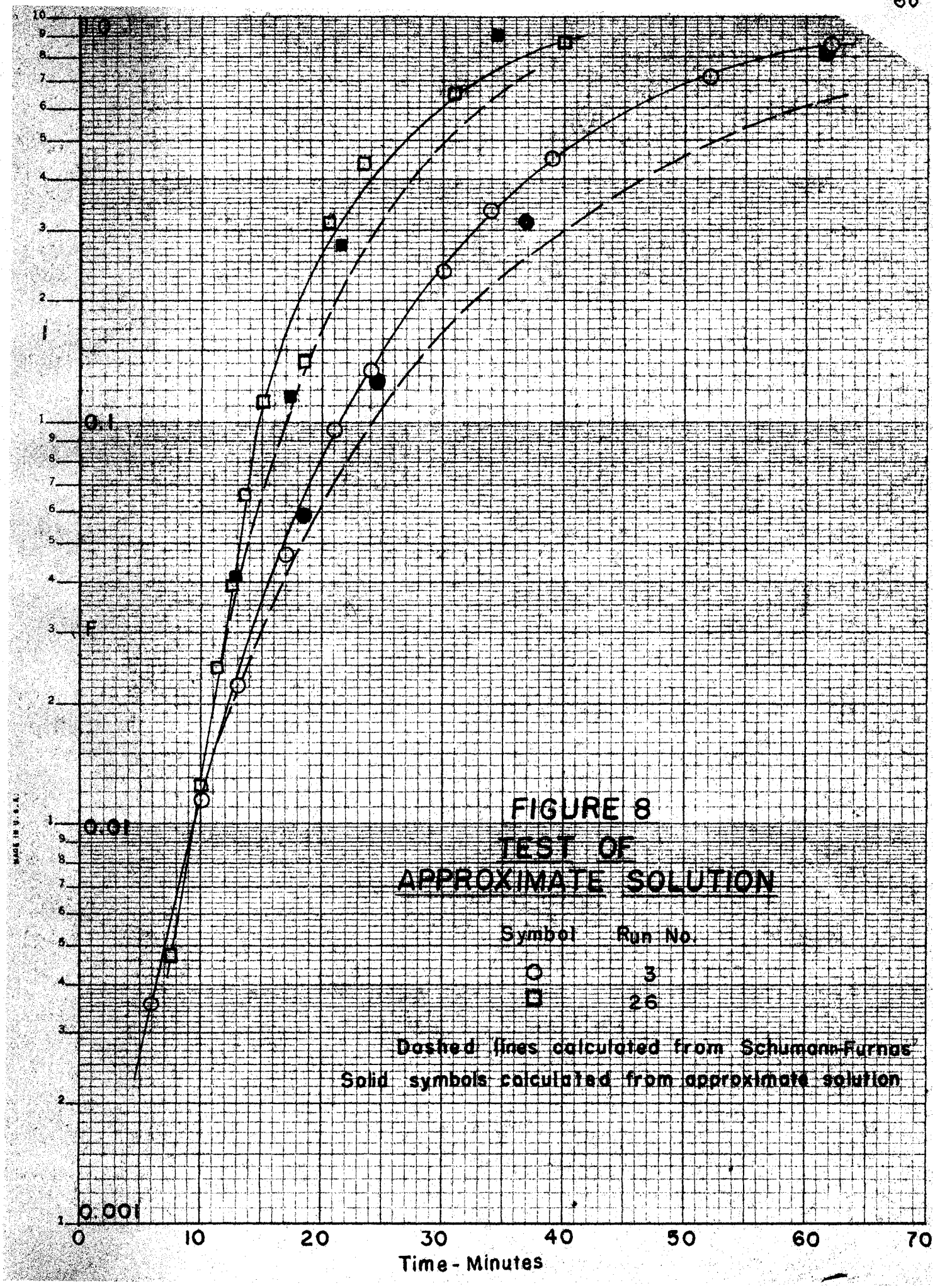

FIGURE 8
TEST OF
APPROXIMATE SOLUTION

Symbol	Run No.
○	3
□	26

Dashed lines calculated from Schumann-Furnas
Solid symbols calculated from approximate solution

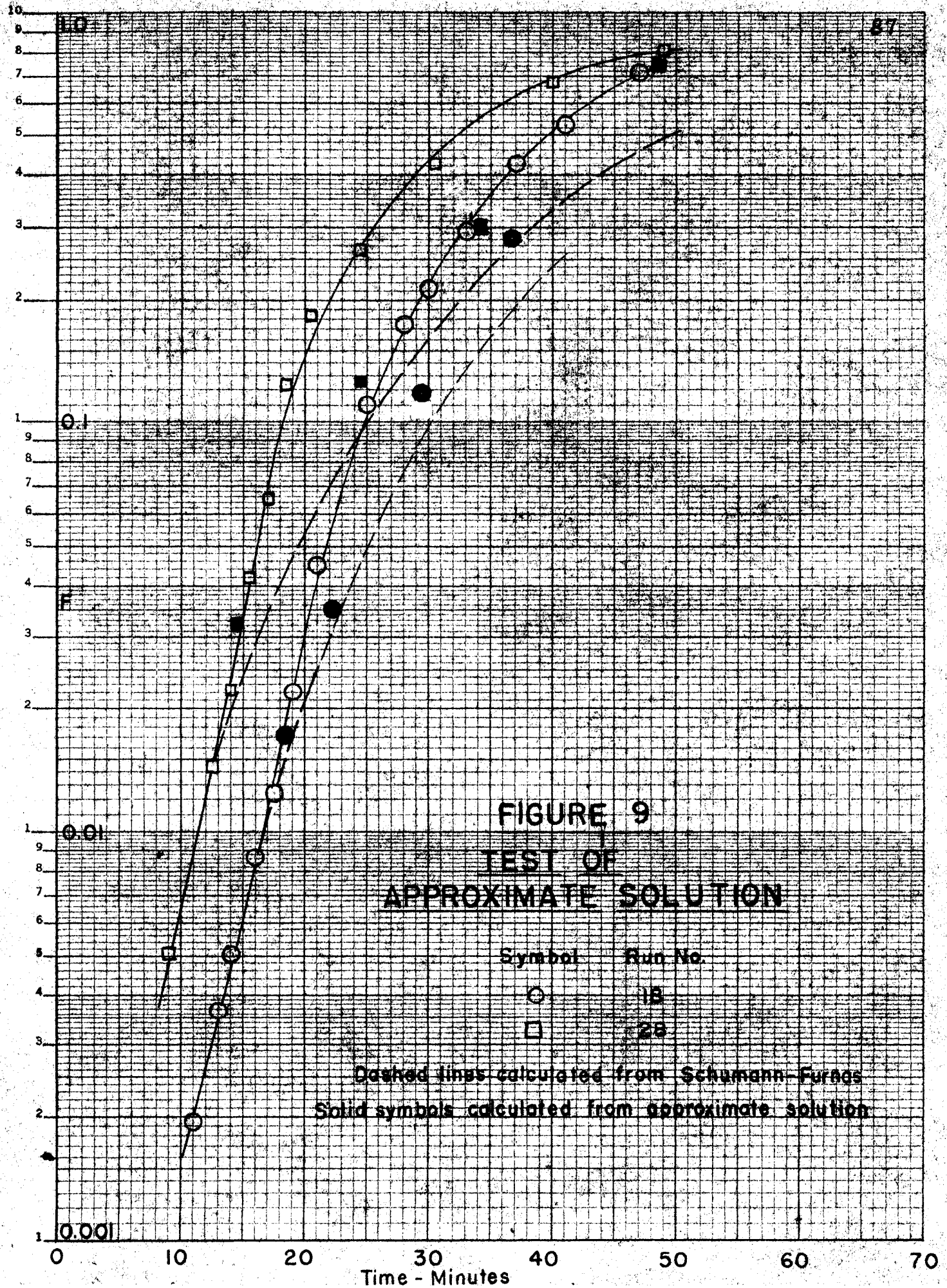

FIGURE 9
TEST OF
APPROXIMATE SOLUTION

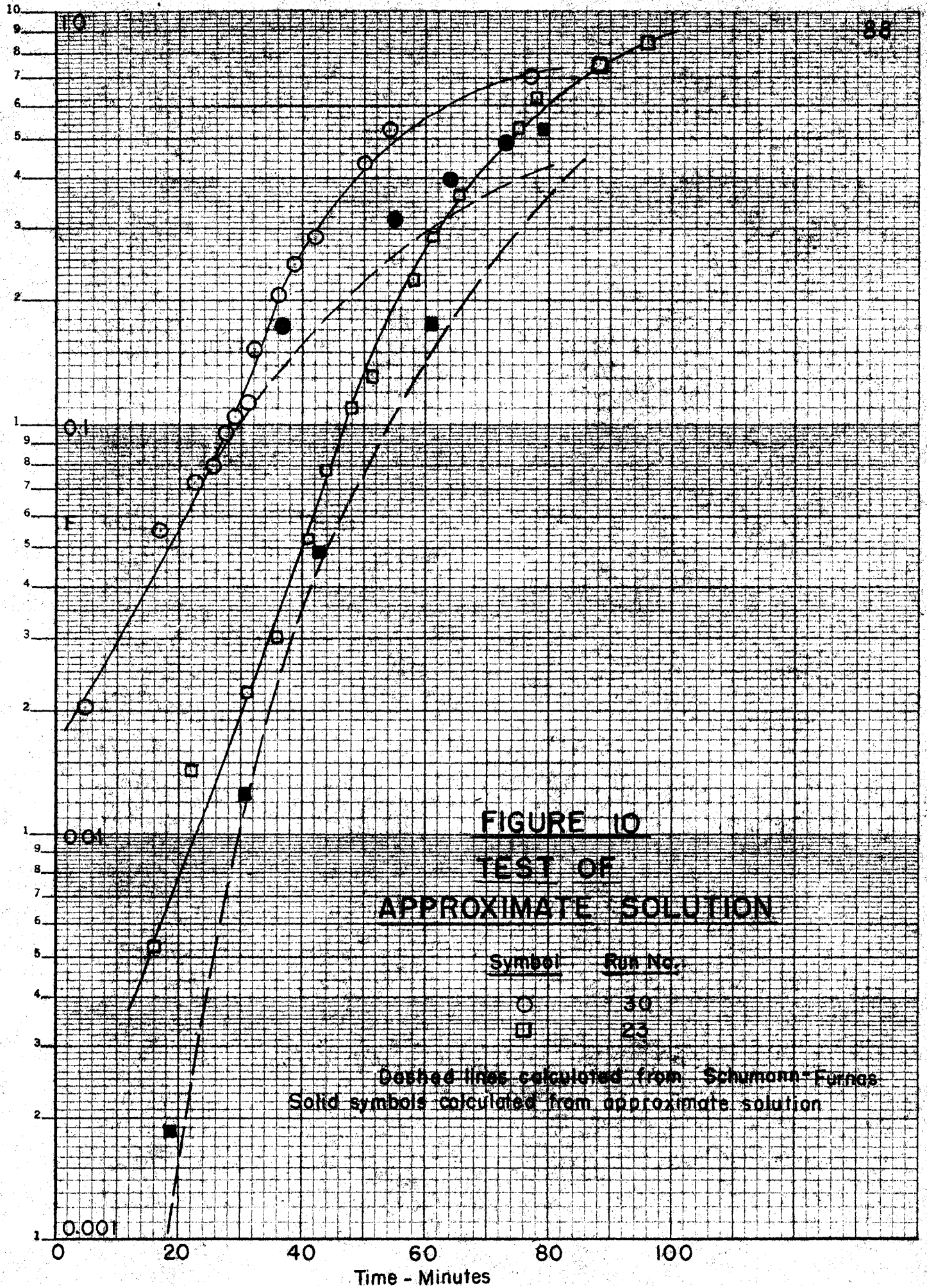

FIGURE 10
TEST OF
APPROXIMATE SOLUTION

Semi-Logarithmic, 3 Cycles X 10 to the inch, 5 to inch accented.
MADE IN U.S.A.

the cumulative amount of moisture picked up by the bed at any time may be determined. Knowing this and the initial moisture content of the bed, the total average moisture content at any time can be calculated. By assuming that the moisture content of the bed was uniform at this value, values of $k_G a$ at various times were calculated from equation 29. Values of X and T were then calculated and the corresponding values of F were read from the Schumann-Furnas charts. Curves calculated in this manner almost always gave values of humidity which were too high. This was attributed to the fact that the moisture content of part of the bed was actually less than the average value calculated in this manner, and that most of the adsorption actually occurs in that portion of the bed having the lowest moisture content. Thus the resistance calculated in this manner is too high. Therefore the results of this test are not conclusive.

Effect of Bed Length

As previously mentioned, the results shown on Fig. 4 and 6 both include runs made on two, three, four, and five inch beds. The fact that one smooth curve was obtained in each case indicates that mass transfer coefficients do not actually vary with bed length as was previously reported. If this were the case, we would expect

to get four distinct curves on Fig. 4 and 6, one for each bed length. Apparently the variation previously observed was due solely to the use of the Schumann-Furnas solution under conditions such that the moisture content of the bed, and hence the resistance to mass transfer, was not uniform. As discussed on p.46, this would give values of X and b which are too high, with the error increasing with increasing bed length.

Because the above tests were made under conditions such that two variables were being changed at once, i.e., bed length and either flow rate or initial moisture content, one additional test on the effect of bed length was attempted. A run was made on a four inch bed, choosing conditions of initial moisture content and flow rate such that the break time was too large to test the data against the Schumann-Furnas solution. A value of B at room temperature during that run was read from Fig. 2. From this and the measured value of H_i^x, the initial moisture content of the bed was calculated. Since the flow rate for this run was the same as that used for the runs represented on Fig. 4, a value of X/z was read directly from this figure. From this, the measured bed length and bulk density, values of X and b were calculated. The adsorption wave was then calculated from equations 48 and 49, as described on p.50. These results are shown in Fig. 10. As before, the points

calculated from equations 48 and 49 lie between the experimental values and those calculated from the Schumann-Furnas solution. Because of the approximate nature of equations 48 and 49, no definite conclusion can be drawn from the results of this particular test.

SUMMARY AND CONCLUSIONS

1. Previous contributions to the theory of the adsorption wave in granular dessicant beds have been reviewed and it has been shown that none of the methods in use are entirely satisfactory for the case where the resistance to either mass transfer or internal diffusion constitutes an appreciable fraction of the total resistance.

2. In the case of mass transfer controlling, the failure of previous methods is attributed to the fact that, for unsteady state operation, the mass transfer coefficient is not constant, as it has always been assumed. As the surface of the particle becomes covered with water molecules, the portion of the surface which is covered may be ineffective for further mass transfer. Thus the resistance to mass transfer is a function of moisture content, and hence of time and distance along the length of the bed. It has been shown how the effective area may be theoretically evaluated as a function of moisture content from knowledge of the adsorption isotherm of the system.

3. In the case of internal diffusion controlling, the failure of previous methods is due to the fact that, as the interior of the particle becomes filled with water molecules the resistance to further movement within the particle is increased. Thus, in this case also, the resistance is a function of moisture content. It has been shown how this

function may be determined empirically.

4. Based on conclusions 2 and 3, two new kinetic relationships have been presented. These have been combined with a material balance to give a new differential equation for the adsorption wave. Two approximate solutions to this differential equation have been obtained, each useful in a different range. These solutions give results which in most cases are a better approximation to experimentally determined adsorption waves than any previous equations. It has been shown that these equations reduce to the Schumann-Furnas solutions at zero time. Based on this fact, a convenient method is presented for testing experimental data and determining which, if any, of the kinetic relationships presented is applicable.

5. An experimental procedure was devised for testing the theories outlined in conclusions 2 and 3. Data was obtained on the system air-water-silica gel, in which the initial moisture content of the beds was varied, holding all other conditions constant. Tests performed on this data confirm the fact that the resistance to mass transfer is a function of the moisture content of the solid.

6. Additional data on this system on the effect of varying flow rate showed that mass transfer is the rate controlling resistance in this system, at least during the initial portion of a run. Tests performed on this data and that discussed in conclusion 5 confirmed the theoreti-

cal relationship between effective mass transfer area and moisture content.

7. Using the theories presented here, it has been shown how it is theoretically possible to calculate quantities which are directly proportional to the mass transfer coefficient k_g and the effective surface area a. It is thus possible to correlate each of these quantities separately against the Reynolds number.

Literature Cited

1. Ahlberg, J., Ind. Eng. Chem. , 31, 988 (1939).

2. Amundsen, N., J. Phys. Chem., 52, 1153 (1948).
ibid, 54, 812 (1950).

3. Anzelius, A., Zeit. fur. Angew. Math. u. Mech., 6, 291 (1926).

4. Brunauer, S., Emmet, J., and Teller, E., J. Amer. Chem. Soc., 60, 309 (1938).

5. DeVault, D., ibid, 65, 532 (1940).

6. Douglass, J., Informal Report No. 10.5-48, National Defemse Research Committee, Office of Scientific Research and Development (1944).

7. Drew, T., Spooner, F., and Douglass, J., ibid.

8. Eagleton, L., "Drying of Air in Fixed Dessicant Beds", Yale University Thesis (D. Sc.) (1950).

9. Furnas, C., Trans. Amer. Inst. Chem. Engrs., 24, 142 (1930).

10. Gamson, B., and Hougen, O., ibid, 39, 1 (1943).

11. Hougen, O., and Dodge, F., "Drying of Gases ", Confidential Report, National Defense Research Committee, Office of Scientific Research and Development (1946).

12. Hougen, O., and Marshall, W., Chem. Eng. Prog., 43, 197 (1947).

13. Hougen, O., and Watson, K., "Chemical Process Principles" p. 1087 , John Wiley and Sons, New York, 1947.

14. Hougen, O, and Watson, K., "Chemical Process Principles Charts", pp. 216, 217. John Wiley and Sons, New York, 1947.

15. Jury, S., Chem. Eng. Prog., 48, 102 (1952).

16. Jury, S,, Anal. Chem., 22, 1536 (1950)

17. Jury, S., "Drying of Gases. The Adsorption Wave in Dessicant Beds", University of Cincinnati Thesis (Ph. D.) (1949)

18. Kayser, R., "Mass Transfer and Variable Area Effects in Fixed Bed Catalytic Converters", University of Cincinnati Thesis (Ph. D.) (1952)

19. Klinkenburg, A., Ind. Eng. Chem., 40, 1992 (1948)

20. Klotz, I., Chem. Rev. 39, 241 (1946)

21. Langmuir, I., J. Amer. Chem. Soc., 38, 2267 (1916)

22. Langmuir, I., ibid, 40, 1361 (1918)

23. Licht, W., "The Adsorption Wave in Beds of Granular Anhydrous Calcium Sulfate", University of Cincinnati Thesis (Ph. D.) (1950)

24. Mecklenburg, W., Z. Elektrochem., 31, 488 (1925)

25. Mecklenburg, W., Kolloid Z., 52, 88 (1930)

26. Gleuckhauf, E., J. Chem. Soc., 149, 1302 (1947)

27. Wicke, E., Kolloid Z., 86, 167-186, 296-313 (1939)

28. Wicke, E., ibid, 93, 129 (1940)

29. Wilke, C., and Hougen, O., Trans. Amer. Inst. Chem. Engrs., 41, 445 (1945)

30. Wilson, J., J. Amer. Chem. Soc., 62, 1583 (1940)

APPENDIX

Sample Calculations

(Run 3)

1. Plot experimental data of H/H_o vs. time in minutes.
2. Select a series of rounded values of F and calculate the corresponding values of H/H_o as follows:

$$H/H_o = F(1 - H_1^*/H_o) + H_1^*/H_o$$

3. For each calculated value of H/H_o read the corresponding time from the plot prepared in step 1, and calculate the square root of the time.
4. For each value of F selected in step 2, obtain the corresponding value of Y from the tables prepared by Licht (23) for this purpose. The results of steps 2 to 4 are presented in the table on page 98.
5. Plot Y vs. $\sqrt{t}$ as shown in Figure 12. From the straight line portion of this curve obtain the slope and intercept:

slope = 0.381 $\qquad$ $b = \text{slope}^2 = 0.145$

intercept = -2.82 $\qquad$ $X = \text{intercept}^2 = 7.95$

6. Using the value of X obtained from step 5 as a first approximation, read the value of T corresponding to each value of F in the table above. For this purpose, a plot was prepared of X vs T for a series of rounded values of F. Plot these values of T against the corresponding time. A straight line through the origin of slope b should result. Repeat this prodedure for

F	H/H_o	t	Y	$\sqrt{t}$
0.001	0.0466	2.8	-2.185	1.67
0.002	0.0475	4.1	-2.035	2.03
0.003	0.0485	5.2	-1.943	2.28
0.005	0.0504	6.7	-1.821	2.59
0.0075	0.0528	8.1		2.85
0.01	0.0551	9.4	-1.645	3.07
0.02	0.0647	12.6	-1.452	3.54
0.03	0.0742	14.6	-1.330	3.82
0.05	0.0933	17.3	-1.163	4.16
0.07	0.112	19.2	-1.044	4.39
0.1	0.141	21.5	-0.906	4.64
0.2	0.236	27.6	-0.595	5.25
0.3	0.332	32.6	-0.371	5.71
0.4	0.427	36.9	-0.179	6.06
0.5	0.552	41.2	0.0	6.41

several values of X, selecting the one giving the best straight line through the origin. Several typical plots are shown on Fig. 13. The best value of X for this run is 9.0 and the value of b obtained from the slope of this line is 0.161.

7. Calculate the mass flow rate and the bulk density of the bed. Mass flow rates were calculated from the following formula, derived from the ideal gas law and the calibration correction for variations in temperature and pressure.

$$G = R\left(\frac{p}{T}\right)^{1/2} 58.1 = 30.0\left(\frac{29.16}{539}\right)^{1/2} 58.1 = 406$$

where G is the mass flow rate in pounds per hour per square foot, R is the uncorrected rotameter reading, p is atmospheric pressure in inches of mercury, and T is room temperature in degrees Rankine.

Bulk density was calculated from the measured weight of dessicant and the dimensions of the bed container as follows.

$$\text{Bulk density} = \frac{16.10 \times 1728}{454 \times 0.785 \times 1^2 \times 2} = 39.0 \ \frac{\text{pounds}}{\text{cu. ft.}}$$

8. Calculate the slope of the adsorption isotherm as follows.

$$B = \frac{XG}{bz\rho_B} = \frac{9.0 \times 406 \times 12}{0.161 \times 60 \times 2 \times 39.0} = 58.0$$

9. From the calculated value of B and the measured value of H_1, calculate the initial moisture content of the bed as follows.

$$W_1 = BH_1^{*} = 58.0 \times 46.1 \times 10^{-6} = 0.00268$$

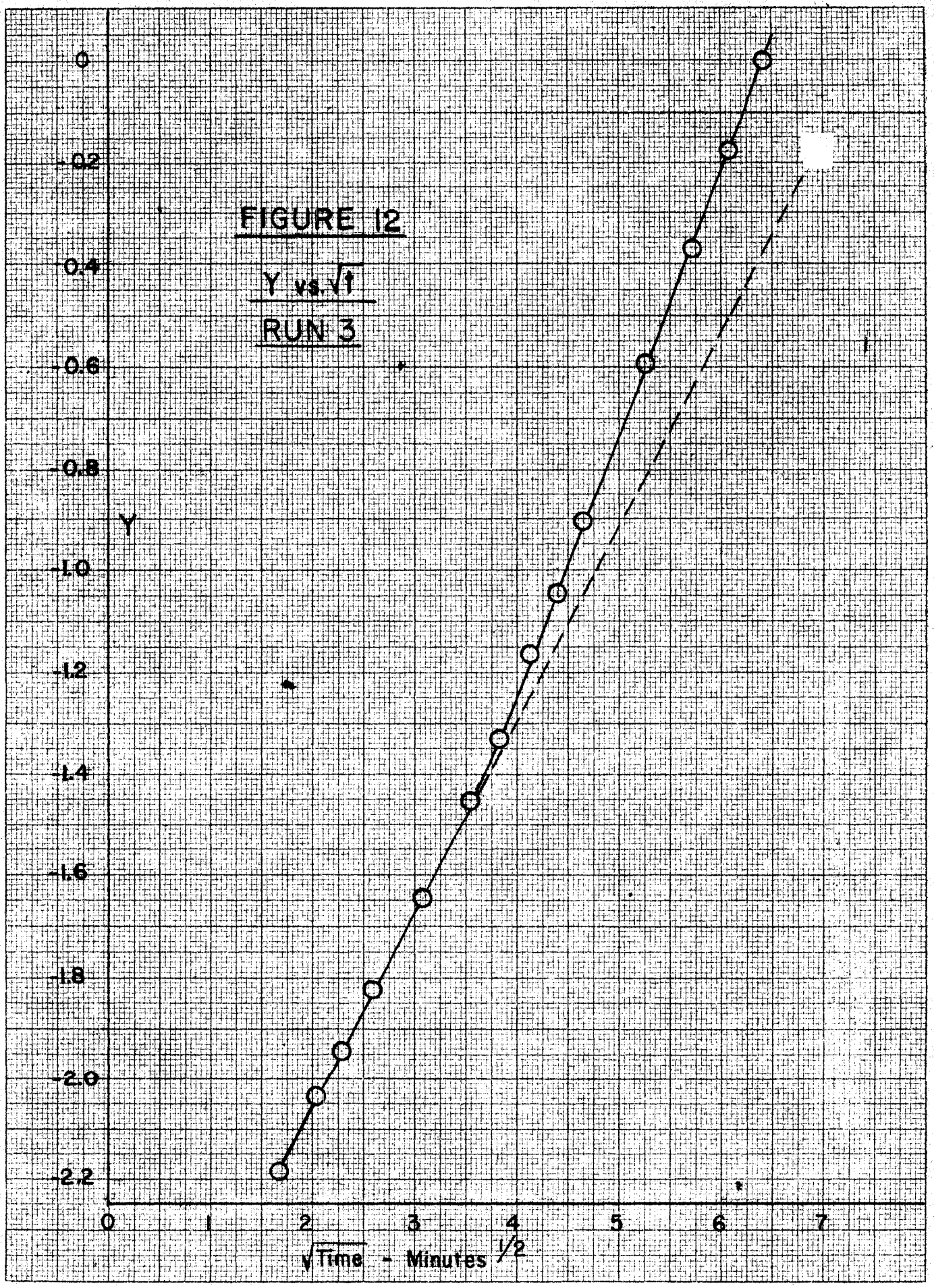

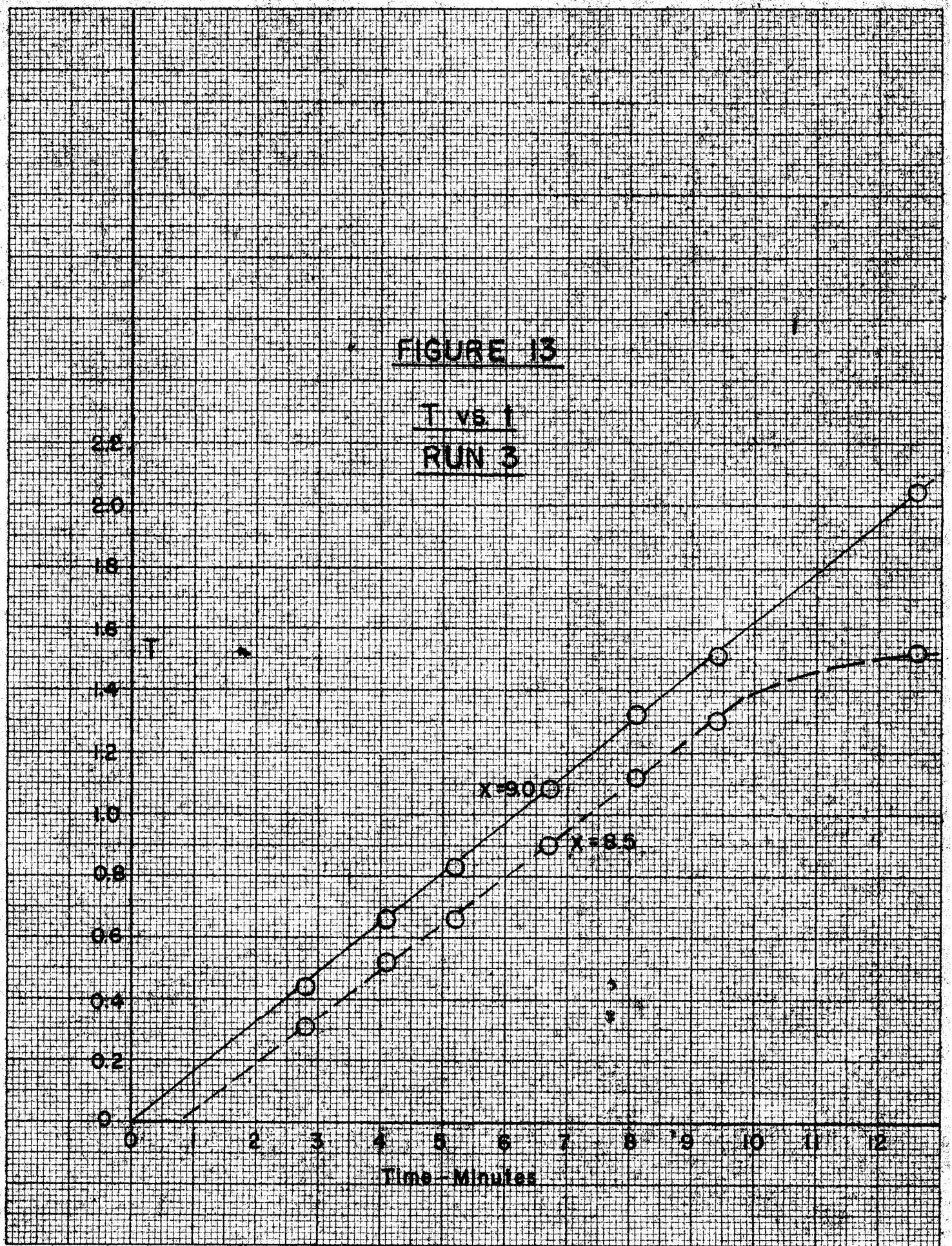

FIGURE 13

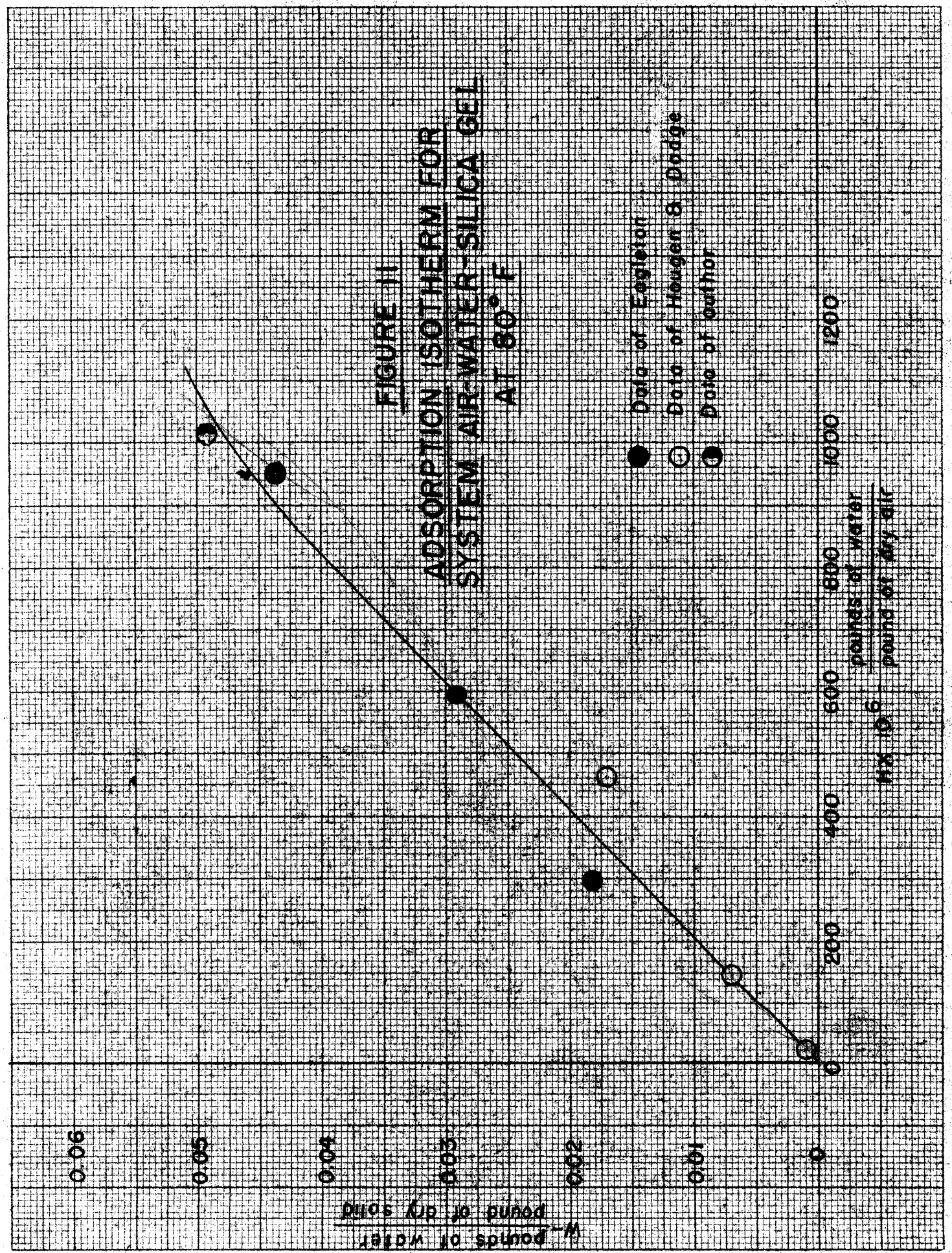

Table II

Summary of Calculated Values
Runs 1-18, 30, 31, 32, 34

Run No.	X	60b $hr.^{-1}$	G $\frac{lbs}{hr\text{-}ft^2}$	z in.	ρ_B $\frac{lbs}{ft^3}$	B $\frac{lbs\ dry\ air}{lb\ dry\ solid}$	W_i $\frac{lbs\ water}{lb\ dry\ solid}$
1	10.2	8.10	406	2	39.0	78.9	0.00101
2	6.2	7.61	409	2	39.0	51.1	0.00500
3	9.0	9.71	406	2	39.0	58.0	0.00268
4	5.0	4.00	403	2	39.0	77.5	0.00860
5	9.0	7.74	405	2	39.0	72.5	0.00212
6	7.1	6.60	404	2	39.0	66.8	0.00415
7	10.5	10.01	406	2	39.0	65.5	0.00122
8	12.2	11.16	405	2	39.0	68.1	0.000940
9	12.5	10.99	409	2	39.0	71.6	0.00133
10	17.5	17.90	407	2	39.0	61.3	0.000403
11	5.6	5.16	407	2	39.0	68.0	0.00570
12	4.6	3.26	405	2	45.0	76.2	0.00900
13	9.2	7.68	405	2	45.0	64.7	0.00212
14	5.8	4.15	407	2	45.0	75.9	0.00655
15	11.3	7.61	405	2	45.0	80.0	0.00170
16	9.4	8.05	408	2	45.0	63.5	0.00223
17	7.5	6.54	405	2	45.0	62.0	0.00292
18	14.9	16.30	410	2	45.0	50.0	0.000413
30	5.4	3.28	405	3	43.0	62.0	0.0111
31	10.1	6.36	409	5	46.4	33.6	0.00721
32	7.1	5.06	406	4	45.0	38.0	0.00764
34	12.2	8.83	405	3	42.9	52.1	0.00318

Table III

Summary of Calculated Values
Runs 19-22, 24-29, 33

Run No.	X	60b $hr.^{-1}$	G $\frac{lbs}{hr\text{-}ft^2}$	z in.	ρ_B $\frac{lbs}{ft^3}$	B $\frac{lbs\ dry\ air}{lb\ dry\ solid}$	W_i $\frac{lbs\ water}{lb\ dry\ solid}$
19	8.0	10.61	470	2	45.0	47.2	0.00197
20	9.3	3.65	272	2	45.0	92.4	0.00408
21	8.2	5.00	338	2	45.0	74.0	0.00356
22	7.7	7.29	541	2	45.0	76.4	0.00409
24	13.4	18.30	671	4	42.5	34.8	0.00259
25	15.0	27.0	802	4	42.5	31.5	0.00228
26	14.5	27.9	935	4	42.5	34.3	0.00256
27	12.5	23.9	1073	4	42.5	39.6	0.00304
28	10.6	12.31	669	3	42.9	53.5	0.00362
29	10.2	15.71	872	3	42.9	52.8	0.00322
33	11.9	24.2	1161	4	45.6	37.6	0.00306

Table IV

Values of F at Low Values of X and T

X \ T	0.3	0.7	1	1.5	2	2.5	3	4	6	8	10
3			0.229								
4	0.0434	0.0861	0.117								
5	0.0191	0.0423	0.0657	0.112							
6	0.00833	0.0206	0.0342	0.0635	0.101						
7	0.00359	0.100	0.0173	0.0348	0.0595	0.0913	0.131				
8	0.00154	0.00476	0.00866	0.0188	0.0342	0.0553	0.0825	0.155	0.346		
9		0.00222	0.00427	0.00995	0.0191	0.0326	0.0509	0.100	0.260		
10			0.00210		0.0105		0.0308	0.0660	0.190		
11			0.00101		0.00565		0.0180	0.0418	0.135		
12			0.000480		0.00303		0.0105	0.0268	0.0940	0.218	
13					0.00161			0.0159	0.0640	0.157	
14					0.000830			0.00960	0.0430	0.113	0.235
15								0.00570	0.0287	0.0800	0.179
16								0.00320	0.0190	0.0560	0.138
17								0.00197	0.0121	0.0400	0.101
18								0.00113	0.00770	0.0280	0.0760
19									0.00468	0.0194	0.0542
20									0.00281	0.0130	0.0388

Table V

Experimental Data for Run 1

Description of Run:*
Bed length - 2 in.
Rotameter reading - 30.0 ft^3./hr.
Room temperature - 78°F.
Barometric pressure - 29.24 in. Hg

Description of Regeneration:
Bath temperature - 200°F.
Pressure of air supply - 40 psig
$H_o = 1012 \times 10^{-6}$

Elapsed time-min.	Surface** temperature °F.	H/H_o	Elapsed time- min.	Surface temperature °F.	H/H_o
0	-66.5	0.01262	30	-28.5	0.157
7	-65.5	0.01411	35	-20.5	0.251
11	-62.5	0.01780	41	-14.5	0.354
15	-59.5	0.0216	45 1/2	- 7.5	0.519
19	-54.0	0.0312	64	* 1.5	0.840
22	-48.5	0.0448	74	+ 3.0	0.909
25	-42.0	0.0694			

Table VI

Experimental Data for Run 2

Description of Run:*
Bed length - 2 in.
Rotameter reading - 30.3 ft^3./hr.
Room temperature - 81°F.
Barometric pressure - 29.10 in. Hg

Description of Regeneration:
Bath temperature - 150°F.
Pressure of air supply - 40 psig
$H_o = 1012 \times 10^{-6}$

Elapsed time-min.	Surface** temperature °F.	H/H_o	Elapsed time-min.	Surface temperature °F.	H/H_o
0	-36.50	0.0965	33 1/2	-10.00	0.454
9 1/2	-31.75	0.1332	37 1/2	- 6.50	0.550
13 1/2	-28.00	0.1620	44 1/2	- 2.50	0.684
17 1/2	-24.50	0.1998	54 1/2	+ 1.50	0.840
21 1/2	-21.00	0.243	74 1/2	+ 3.50	0.934
25 1/2	-16.50	0.316			

* Data on bulk density of these beds appear on p. III. Pressure of air supply for all runs was 40 psig., corresponding to $H_o = 1012 \times 10^{-6}$. All rotameter readings are uncorrected readings.
** All surface deposits were ice unless otherwise noted.

Table VII

Experimental Data for Run 3

Description of Run:*
Bed length - 2 in.
Rotameter reading - 30.0 ft^3./hr.
Room temperature - 79°F.
Barometric pressure - 29.16 in. Hg

Description of Regeneration:
Bath temperature - 170°F.
Pressure of air supply - 40 psig
$H_o = 1012 \times 10^{-6}$

Elapsed time-min.	Surface** temperature °F.	H/H_o	Elapsed time-min.	Surface temperature °F.	H/H_o
0	-48.25	0.0456	30	-19.0	0.273
6	-47.0	0.0490	34	-14.0	0.364
10	-45.0	0.0565	39	- 9.0	0.477
13	-42.5	0.0668	52	- 1.0	0.729
17	-37.5	0.0906	62	+ 2.0	0.861
21	-31.0	0.137	77	+ 3.5	0.934
24	-27.0	0.172			

Table VIII

Experimental Data for Run 4

Description of Run:*
Bed length - 2 in.
Rotameter reading - 29.5 ft^3./hr.
Room temperature - 75°F.
Barometric pressure - 29.50 in. Hg

Description of Regeneration:
Bath temperature - 140°F.
Pressure of air supply - 40 psig
$H_o = 1012 \times 10^{-6}$

Elapsed time-min.	Surface** temperature °F.	H/H_o	Elapsed time-min.	Surface temperature °F.	H/H_o
0	-34.5	0.110	37	- 9.0	0.472
7	-31.5	0.135	44	- 5.5	0.579
12 1/2	-28.75	0.155	48	- 3.5	0.649
15 1/2	-26.75	0.174	57	0	0.774
22	-22.5	0.226	65	+ 2.0	0.861
29	-16.5	0.316	73	+ 2.3	0.875
33	-14.0	0.364	90	+ 4.0	0.958

* Data on bulk density of these beds appear on p. 111.
** All surface deposits were ice unless otherwise noted.

Table IX

Experimental Data for Run 5

Description of Run:*
Bed length - 2 in.
Rotameter reading - 29.8 ft^3./hr.
Room temperature - 79°F.
Barometric pressure - 29.56 in. Hg

Description of Regeneration:
Bath temperature - 180°F.
Pressure of air supply - 40 psig.
$H_o = 1012 \times 10^{-6}$

Elapsed time-min.	Surface** temperature °F.	H/H_o	Elapsed time-min.	Surface temperature °F.	H/H_o
0	-55.0	0.0288	28	-27.0	0.172
6	-54.0	0.0312	36	-16.0	0.324
11	-51.5	0.0372	41	-10.5	0.442
16	-47.0	0.0490	56	- 1.0	0.729
20	-40.0	0.0779	68	+ 2.0	0.860
23	-34.0	0.114	76	+ 2.7	0.891

Table X

Experimental Data for Run 6

Description of Run:*
Bed length - 2 in.
Rotameter reading - 29.7 ft^3./hr.
Room temperature - 78°F.
Barometric pressure - 29.42 in. Hg

Description of Regeneration:
Bath temperature - 160°F.
Pressure of air supply - 40 psig.
$H_o = 1012 \times 10^{-6}$

Elapsed time-min.	Surface** temperature °F.	H/H_o	Elapsed time-min.	Surface temperature °F.	H/H_o
0	-43.75	0.0614	33	-16.0	0.324
7	-41.5	0.0715	40	-11.0	0.430
11	-39.5	0.0802	52	- 2.5	0.684
14	-36.5	0.0965	59	+ 1.0	0.815
19	-32.5	0.126	71	+ 2.7	0.891
24	-27.0	0.172			

* Data on bulk density of these beds appear on p.///.
** All surface deposits were ice unless otherwise noted.

Table XI

Experimental Data for Run 7

Description of Run:*
Bed length - 2 in.
Rotameter reading - 29.7 ft^3./hr.
Room temperature - 75°F.
Barometric pressure - 29.44 in. Hg

Description of Regeneration:
Bath temperature - 190°F.
Pressure of air supply - 40 psig.
$H_o = 1012 \times 10^{-6}$

Elapsed time-min.	Surface** temperature °F.	H/H_o	Elapsed time-min.	Surface temperature °F.	H/H_o
0	-62.0	0.0184	26	-36.5	0.0965
5	-61.25	0.0193	34	-24.0	0.206
9	-59.0	0.0222	38 1/2	-18.0	0.290
13	-54.75	0.0294	46	-10.0	0.454
17	-50.5	0.0399	53	- 4.0	0.631
21	-44.5	0.0584	76	+ 2.3	0.875

Table XII

Experimental Data for Run 8

Description of Run:*
Bed length - 2 in.
Rotameter reading - 29.8 ft^3./hr.
Room temperature - 79°F.
Barometric pressure - 29.48 in. Hg

Description of Regeneration:
Bath temperature - 210°F.
Pressure of air supply - 40 psig.
$H_o = 1012 \times 10^{-6}$

Elapsed time-min.	Surface** temperature °F.	H/H_o	Elapsed time-min.	Surface temperature °F.	H/H_o
0	-66.0	0.0136	25	-38.0	0.0876
10	-64.0	0.0157	31	-25.5	0.188
13	-62.0	0.0184	40	-15.5	0.334
16	-59.0	0.0222	55	- 5.0	0.595
19	-54.25	0.0306	82	+ 1.25	0.827

* Data on bulk density of these beds appear on p.///.
** All surface deposits were ice unless otherwise noted.

Table XIII

Experimental Data for Run 9

Description of Run:*
Bed length - 2 in.
Rotameter Reading - 30.0 ft.^{3}/hr.
Room temperature - 78 F.
Barometric pressure - 29.38 in. Hg

Description of Regeneration:
Bath temperature - 200°F
Pressure of air supply - 40 psig.
$H_o = 1012 \times 10^{-6}$

Elapsed time-min.	Surface** temperature F	H/H_o	Elapsed time-min.	Surface temperature F	H/H_o
0	-62.0	0.0184	26	-31.5	0.135
8	-61.5	0.0191	29	-26.5	0.177
11	-60.5	0.0204	35	-19.0	0.272
15	-58.0	0.0238	39	-13.0	0.385
17	-55.25	0.0284	43	- 9.25	0.471
19	-53.5	0.0323	51	- 4.0	0.632
21	-51.0	0.0386	62	+0.5	0.795
22 1/2	-44.0	0.0602	76	+ 2.3	0.875

Table XIV

Experimental Data for Run 10

Description of Run:*
Bed length - 2 in.
Rotameter reading - 29.9 ft.^{3}/hr.
Room temperature - 76.5 F
Barometric pressure - 29.38 in. Hg

Description of Regeneration:
Bath temperature - 230°F
Pressure of air supply - 40 psig.
$H_o = 1012 \times 10^{-6}$

Elapsed time-min.	Surface temperature F	H/H_o	Elapsed time-min.	Surface temperature F	H/H_o
0	-76.0	0.00650	24	-42.5	0.0668
11	-75.0	0.00705	28	-34.0	0.114
14	-73.0	0.00815	32	-26.5	0.177
16	-70.5	0.00978	34	-24.0	0.206
19	-63.0	0.0171	37	-19.5	0.266
21	-55.5	0.0280	42	-12.5	0.396
22	-50.5	0.0399	47	- 8.0	0.502

* Data on bulk density of these beds appear on p.111 .
** All surface deposits were ice unless otherwise noted.

Table XV

Experimental Data for Run 11

Description of Run:*
Bed length - 2 in.
Rotameter reading - 29.8 ft^3./hr.
Room temperature - 75°F.
Barometric pressure - 29.42 in. Hg

Description of Regeneration:
Bath temperature - 145°F.
Pressure of air supply - 40 psig.
$H_o = 1012 \times 10^{-6}$

Elapsed time-min.	Surface** temperature °F.	H/H_o	Elapsed time-min.	Surface temperature °F.	H/H_o
0	-39.0	0.0826	26	-20.5	0.251
2	-38.0	0.0876	29	-18.0	0.290
5	-36.5	0.0965	33 1/2	-13.25	0.378
7	-35.0	0.106	37	-10.0	0.454
15	-30.5	0.141	41	- 7.5	0.519
18 1/2	-28.0	0.162	52	- 3.0	0.664
21 1/2	-25.5	0.188	59	0.0	0.774

* Data on bulk density of these beds appear on p. 111.
** All surface deposits were ice unless otherwise noted.

Data on weight of bed for runs 1-11:

Wt. of tare + dessicant -	40.04 gms.
Wt. of tare -	23.90
Wt. of dessicant -	16.10 gms.

Table XVI

Experimental Data for Run 12

Description of Run:*
Bed length - 2 in.
Rotameter reading - 29.8 $ft.^3$/hr.
Room temperature - 76°F.
Barometric pressure - 29.40 in. Hg

Description of Regeneration:
Bath temperature - 140°F.
Pressure of air supply - 40 psig.
$H_o = 1012 \times 10^{-6}$

Elapsed time-min.	Surface** temperature °F.	H/H_o	Elapsed time-min.	Surface temperature °F.	H/H_o
0	-33.5	0.116	33	-14.0	0.364
4	-31.5	0.135	38	-10.75	0.436
7 1/2	-30.0	0.145	46	- 5.0	0.595
12 1/2	-28.0	0.162	51	- 2.0	0.700
15	-26.5	0.177	62	+ 1.5	0.840
24	-22.0	0.232	80	+ 3.5	0.934
28	-18.5	0.282			

Table XVII

Experimental Data for Run 13

Description of Run:*
Bed length - 2 in.
Rotameter reading - 29.8 $ft.^3$/hr.
Room temperature - 75°F.
Barometric pressure - 29.28 in. Hg

Description of Regeneration:
Bath temperature - 170°F.
Pressure of air supply - 40 psig.
$H_o = 1012 \times 10^{-6}$

Elapsed time-min.	Surface** temperature °F.	H/H_o	Elapsed time-min.	Surface temperature °F.	H/H_o
0	-53.5	0.0323	34	-26.0	0.182
9	-52.0	0.0358	36 1/2	-22.5	0.226
12 1/2	-49.0	0.0436	39 1/2	-18.5	0.282
16 1/2	-47.0	0.0490	43 1/2	-14.0	0.364
21	-43.5	0.0624	46	-10.0	0.454
25	-41.0	0.0735	55	- 5.0	0.595
29	-37.0	0.0930	64	- 0.5	0.752

* Data on bulk density of these beds appear on p.117.
** All surface deposits were ice unless otherwise noted.

Table XVIII

Experimental Data for Run 14

Description of Run:*
Bed length - 2 in.
Rotameter reading - 29.9 ft^3./hr.
Room temperature - 78°F.
Barometric pressure - 29.38 in. Hg

Description of Regeneration:
Bath temperature - 170°F.
Pressure of air supply - 10 psig
$H_o = 2260 \times 10^{-6}$

Elapsed time-min.	Surface** temperature °F.	H/H_o	Elapsed time-min.	Surface temperature °F.	H/H_o
0	-38.5	0.0851	27	-21.0	0.243
7	-36.0	0.0996	31	-16.5	0.316
11	-34.5	0.110	34 1/2	-13.0	0.385
16	-32.5	0.126	38	-11.0	0.430
18 1/2	-30.5	0.141	43 1/2	- 6.5	0.550
20 1/2	-29.0	0.152	49 1/2	- 4.0	0.632
22	-27.0	0.172	58	+ 0.5	0.795
25	-24.0	0.206	70	+ 3.0	0.909

Table XIX

Experimental Data for Run 15

Description of Run:*
Bed length - 2 in.
Rotameter reading - 29.6 ft^3./hr.
Room temperature - 74°F.
Barometric pressure - 29.48 in. Hg

Description of Regeneration:
Bath temperature - 170°F.
Pressure of air supply - 80 psig
$H_o = 583 \times 10^{-6}$

Elapsed time-min.	Surface** temperature °F.	H/H_o	Elapsed time-min.	Surface temperature °F.	H/H_o
0	-60.0	0.0210	30 1/2	-33.5	0.117
3	-60.0	0.0210	34	-27.5	0.167
7	-59.5	0.0216	37	-23.5	0.212
13	-58.0	0.0238	40 1/2	-17.5	0.298
16 1/2	-56.5	0.0261	44 1/2	-13.0	0.385
19	-55.0	0.0288	51	- 8.0	0.502
21	-53.5	0.0323	61	- 2.0	0.700
23	-48.5	0.0450	67	- 0.5	0.752
26	-42.5	0.0669	81	+ 1.0,	0.816

* Data on bulk density of these beds appear on p.117.
** All surface deposits were ice unless otherwise noted.

Table XX

Experimental Data for Run 16

Description of Run:*
Bed length - 2 in.
Rotameter reading - 30.1 ft^3./hr.
Room temperature - 81.5°F.
Barometric pressure - 29.42 in. Hg

Description of Regeneration:
Bath temperature - 170°F.
Pressure of air supply - 60 psig
$H_o = 739 \times 10^{-6}$

Elapsed time-min.	Surface** temperature °F.	H/H_o	Elapsed time-min.	Surface temperature °F.	H/H_o
0	-52.5	0.0347	22	-38.0	0.0876
4	-52.0	0.0358	24 1/2	-33.5	0.118
8	-50.5	0.0399	26 1/2	-28.0	0.162
11 1/2	-50.0	0.0412	28	-25.5	0.188
14 1/2	-47.0	0.0490	33	-18.5	0.282
17	-45.0	0.0565	35 1/2	-15.0	0.344
18	-43.5	0.0624	39	-10.5	0.441
20	-41.0	0.0736	45	- 7.5	0.519

Table XXI

Experimental Data for Run 17

Description of Run:*
Bed length - 2 in.
Rotameter reading - 29.6 ft^3./hr.
Room temperature - 78°F.
Barometric pressure - 29.73 in. Hg

Description of Regeneration:
Bath temperature - 170°F.
Pressure of air supply - 25 psig
$H_o = 1400 \times 10^{-6}$

Elapsed time-min.	Surface** temperature °F.	H/H_o	Elapsed time-min.	Surface temperature °F.	H/H_o
0	-47.5	0.0476	27 1/2	-29.0	0.152
3	-47.0	0.0490	30	-25.25	0.190
7	-45.0	0.0565	34	-19.5	0.266
10	-43.0	0.0644	37	-15.5	0.344
14 1/2	-41.5	0.0715	40	-13.0	0.385
16	-40.25	0.0768	43	-10.0	0.454
19	-38.0	0.0876	48	- 6.5	0.550
21 1/2	-35.5	0.103	55	- 2.0	0.700
25	-33.0	0.120	71	+ 1.5	0.838

* Data on bulk density of these beds appear on p.117.
** All surface deposits were ice unless otherwise noted.

Table XXII

Experimental Data for Run 18

Description of Run:*
Bed length - 2 in.
Rotameter reading - 30.5 ft^3./hr.
Room temperature - 87°F.
Barometric pressure - 29.30 in. Hg

Description of Regeneration:
Bath temperature - 220°F
Pressure of air supply - 40 psig
$H_o = 1012 \times 10^{-6}$

Elapsed time-min.	Surface** temperature °F.	H/H_o	Elapsed time-min.	Surface temperature °F.	H/H_o
0	-73.0	0.00815	21	-46.0	0.0529
3	-73.0	0.00815	25	-33.5	0.118
9	-71.5	0.00907	28	-26.0	0.182
11	-70.0	0.0101	30	-23.0	0.218
13	-68.0	0.0118	33	-17.5	0.298
14	-66.5	0.0131	37	-11.0	0.430
16	-63.25	0.0167	41	- 7.0	0.534
17 1/2	-60.5	0.0204	47	- 1.5	0.715
19	-54.5	0.0300			

Table XXIII

Experimental Data for Run 19

Description of Run:*
Bed length - 2 in.
Rotameter reading - 35.0 ft^3./hr.
Room temperature - 84°F.
Barometric pressure - 29.31 in. Hg

Description of Regeneration:
Bath temperature - 170°F.
Pressure of air supply - 40 psig
$H_o = 1012 \times 10^{-6}$

Elapsed time-min.	Surface** temperature °F.	H/H_o	Elapsed time-min.	Surface temperature °F.	H/H_o
0	-50.0	0.0412	20 1/2	-22.5	0.225
5	-47.5	0.0476	23 1/2	-18.0	0.290
8 1/2	-43.5	0.0624	26 1/2	-14.0	0.364
11	-41.5	0.0715	30 1/2	- 8.0	0.502
13	-37.5	0.0905	35 1/2	- 4.5	0.614
15	-34.5	0.110	43	0.0	0.773
16 1/2	-31.5	0.135	75	+ 2.7	0.891
18	-28.25	0.160			

* Data on bulk density of these beds appear on p. 117.
** All surface deposits were ice unless otherwise noted.

Table XXIV

Experimental Data for Run 20

Description of Run:*
Bed length - 2 in.
Rotameter reading - 20.0 ft^3./hr.
Room temperature - 77.5°F.
Barometric pressure - 29.46 in. Hg

Description of Regeneration:
Bath temperature - 170°F.
Pressure of air supply - 40 psig
$H_o = 1012 \times 10^{-6}$

Elapsed time-min.	Surface** temperature °F.	H/H_o	Elapsed time-min.	Surface temperature °F.	H/H_o
0	-49.0	0.0436	48	-31.0	0.137
6	-49.0	0.0436	52 1/2	-26.5	0.177
12	-48.5	0.0450	54	-25.0	0.194
20	-47.0	0.0490	59	-19.5	0.266
26	-46.0	0.0529	63	-17.0	0.307
31	-44.75	0.0575	66 1/2	-12.5	0.396
36	-43.5	0.0624	74	- 9.0	0.476
40	-41.0	0.0736	79	- 6.5	0.550
42	-39.25	0.0815	96	- 0.5	0.752
44 1/2	-36.5	0.0965			

Table XXV

Experimental Data for Run 21

Description of Run:*
Bed length - 2 in.
Rotameter reading - 25.0 ft^3./hr.
Room temperature - 82°F.
Barometric pressure - 29.50 in. Hg

Description of Regeneration:
Bath temperature - 170°F.
Pressure of air supply - 40 psig
$H_o = 1012 \times 10^{-6}$

Elapsed time-min.	Surface** temperature °F.	H/H_o	Elapsed time-min.	Surface temperature °F.	H/H_o
0	-47.5	0.0476	32 1/2	-29.0	0.152
2	-47.5	0.0476	35 1/2	-24.0	0.206
7	-46.0	0.0529	39 1/2	-19.5	0.266
14	-45.0	0.0565	43	-16.5	0.316
18	-43.5	0.0624	46	-13.5	0.374
21	-42.0	0.0694	51 1/2	- 9.0	0.476
24	-39.5	0.0803	57	- 5.5	0.579
26	-37.5	0.0906	64	0.0	0.774
28 1/2	-35.0	0.106	77	+ 2.3	0.874
30 1/2	-32.5	0.126			

* Data on bulk density of these beds appear on p.117.
** All surface deposits were ice unless otherwise noted.

Table XXVI

Experimental Data for Run 22

Description of Run:
Bed length - 2 in.
Rotameter reading - 40.0 ft^3./hr.
Room temperature - 82°F.
Barometric pressure - 29.52 in. Hg

Description of Regeneration:
Bath temperature - 170°F.
Pressure of air supply - 40 psig
$H_o = 1012 \times 10^{-6}$

Elapsed time-min.	Surface* temperature °F.	H/H_o	Elapsed time-min.	Surface temperature °F.	H/H_o
0	-46.0	0.0529	16 1/2	-30.0	0.145
4 1/2	-45.0	0.0565	19	-26.5	0.177
7 1/2	-44.0	0.0602	21	-22.5	0.226
9	-43.0	0.0644	24	-17.5	0.298
12	-38.5	0.0851	28	-13.25	0.380
14	-35.5	0.103	31	- 9.5	0.465

* All surface deposits were ice unless otherwise noted.

Data on weight of bed for runs 12-22:

Wt. of tare + dessicant -	40.04 gms.
Wt. of tare -	21.52
Wt. of dessicant -	18.52 gms.

Table XXVII

Experimental Data for Run 23

Description of Run:*
Bed length - 4 in.
Rotameter reading - 30.4 ft^3./hr.
Room temperature - 85°F.
Barometric pressure - 29.38 in. Hg

Description of Regeneration:
Bath temperature - 170°F.
Pressure of air supply - 40 psig.
$H_o = 1012 \times 10^{-6}$

Elapsed time-min.	Surface** temperature °F.	H/H_o	Elapsed time-min.	Surface temperature °F.	H/H_o
0	-43.0	0.0644	51 1/2	-25.5	0.188
8	-43.0	0.0644	58	-19.0	0.273
16	-42.0	0.0694	61 1/2	-15.5	0.334
22	-40.0	0.0779	65 1/2	-12.0	0.406
31	-38.5	0.0851	75	- 6.0	0.565
36	-37.0	0.0930	78	- 3.5	0.649
41	-34.0	0.114	88	0.0	0.774
44	-31.0	0.137	96	+ 2.0	0.861
48	-27.5	0.167			

Table XXVIII

Experimental Data for Run 24

Description of Run:*
Bed length - 4 in.
Rotameter reading - 50.0 ft^3./hr.
Room temperature - 87°F.
Barometric pressure - 29.42 in. Hg

Description of Regeneration:
Bath temperature - 170°F.
Pressure of air supply - 40 psig.
$H_o = 1012 \times 10^{-6}$

Elapsed time-min.	Surface** temperature °F.	H/H_o	Elapsed time-min.	Surface temperature °F.	H/H_o
0	-41.0	0.0735	25	-25.5	0.188
11 1/2	-39.5	0.0802	27	-22.0	0.232
13	-38.0	0.0876	30 1/2	-17.75	0.303
15	-37.0	0.0930	35	-12.5	0.396
17	-35.5	0.103	39 1/2	- 7.0	0.534
19 1/2	-32.75	0.128	51	0.0	0.773
21 1/2	-30.0	0.145	59	+ 2.3	0.874

* Data on bulk density of these beds appear on p.120.
** All surface deposits were ice unless otherwise noted.

Table XXIX

Experimental Data for Run 25

Description of Run:*
Bed length - 4 in.
Rotameter reading - 60.0 ft^3./hr.
Room temperature - 87.5°F.
Barometric pressure - 29.45 in. Hg

Description of Regeneration:
Bath temperature - 170°F.
Pressure of air supply - 40 psig.
$H_o = 1012 \times 10^{-6}$

Elapsed time-min.	Surface** temperature °F.	H/H_o	Elapsed time-min.	Surface temperature °F.	H/H_o
0	-41.5	0.0715	23	-17.5	0.298
7	-41.0	0.0735	26	-13.5	0.374
11	-38.5	0.0851	28	-10.75	0.435
13	-36.0	0.0995	33 1/2	- 5.5	0.580
14 1/2	-34.0	0.113	38	- 1.25	0.721
16	-30.5	0.141	42 1/2	+ 0.5	0.795
18	-26.0	0.182	46	+ 2.0	0.860
20 1/2	-22.0	0.232			

Table XXX

Experimental Data for Run 26

Description of Run:*
Bed length - 4 in.
Rotameter reading - 70.0 ft^3./hr.
Room temperature - 88°F.
Barometric pressure - 29.38 in. Hg

Description of Regeneration:
Bath temperature + 170°F.
Pressure of air supply - 40 psig.
$H_o = 1012 \times 10^{-6}$

Elapsed time-min.	Surface** temperature °F.	H/H_o	Elapsed time-min.	Surface temperature °F.	H/H_o
0	-41.0	0.0735	15	-26.5	0.177
4	-41.0	0.0735	18 1/2	-17.5	0.298
7 1/2	-40.0	0.0779	20 1/2	-14.0	0.363
10	-38.5	0.0851	23 1/2	- 9.0	0.477
11 1/4	-36.5	0.0965	31	- 2.5	0.683
12 1/2	-34.5	0.110	33 1/2	- 0.5	0.751
13 1/2	-31.5	0.135	40	+ 2.3	0.874

* Data on bulk density of these beds appear on p.120.
** All surface deposits were ice unless otherwise noted.

Table XXXI

Experimental Data for Run 27

Description of Run:
Bed length - 4 in.
Rotameter reading - 80.0 ft^3./hr.
Room temperature - 86°F.
Barometric pressure - 29.58 in. Hg

Description of Regeneration:
Bath temperature - 170°F.
Pressure of air supply - 40 psig
$H_o = 1012 \times 10^{-6}$

Elapsed time-min.	Surface** temperature °F.	H/H_o	Elapsed time-min.	Surface temperature °F.	H/H_o
0	-40.5	0.0757	15 1/2	-22.0	0.232
6 1/2	-39.5	0.0802	17 1/2	-15.5	0.334
10 1/2	-36.0	0.0995	21	-10.5	0.441
12 1/2	-30.0	0.145	24	- 5.0	0.595
14	-27.0	0.172	32	+ 0.5	0.795

Data on weight of bed for runs 23-27:

Wt. of tare + dessicant -	82.58 gms.
Wt. of tare -	47.58
Wt. of dessicant -	35.00 gms.

Table XXXII

Experimental Data for Run 28

Description of Run:*
Bed length - 3 in.
Rotameter reading - 50.0 ft^3./hr.
Room temperature - 86°F.
Barometric pressure - 29.50 in. Hg

Description of Regeneration:
Bath temperature - 170°F.
Pressure of air supply - 40 psig
$H_o = 1012 \times 10^{-6}$

Elapsed time-min.	Surface** temperature °F.	H/H_o	Elapsed time-min.	Surface temperature °F.	H/H_o
0	-42.5	0.0668	18 1/2	-26.0	0.182
9	-41.5	0.0715	20 1/2	-21.5	0.238
12 1/2	-39.5	0.0802	24 1/2	-16.5	0.316
14	-38.0	0.0876	30 1/2	- 9.5	0.465
15 1/2	-35.0	0.106	40	- 2.0	0.700
17	-31.0	0.137	49	+ 1.0	0.816

* Data on bulk density of these beds appear on p. 123.
** All surface deposits were ice unless otherwise noted.

Table XXXIII

Experimental Data for Run 29

Description of Run:*
Bed length - 3 in.
Rotameter reading - 65.0 $ft.^3/hr.$
Room temperature - 83°F.
Barometric pressure - 29.38 in. Hg

Description of Regeneration:
Bath temperature - 170°F.
Pressure of air supply - 40 psig.
$H_o = 1012 \times 10^{-6}$

Elapsed time-min.	Surface** temperature °F.	H/H_o	Elapsed time-min.	Surface temperature °F.	H/H_o
0	-44.0	0.0602	13	-30.0	0.145
7	-42.5	0.0668	14 1/2	-25.0	0.194
8 1/2	-41.5	0.0715	16	-21.0	0.243
9 1/2	-40.0	0.0779	18	-18.0	0.290
10 1/2	-37.0	0.0930	20 1/2	-15.0	0.344
12	-34.0	0.114			

Table XXXIV

Experimental Data for Run 30

Description of Run:*
Bed length - 3 in.
Rotameter reading - 30.2 $ft.^3/hr.$
Room temperature - 84°F.
Barometric pressure - 29.38 in. Hg

Description of Regeneration:
Bath temperature - 140°F.
Pressure of air supply - 40 psig.
$H_o = 1012 \times 10^{-6}$

Elapsed time-min.	Surface** temperature °F.	H/H_o	Elapsed time-min.	Surface temperature °F.	H/H_o
0	-26.5	0.172	32	-17.5	0.298
5	-25.5	0.188	36	-15.0	0.344
17	-23.0	0.218	38 1/2	-13.5	0.374
22 1/2	-22.0	0.232	42	-12.0	0.406
25 1/2	-21.5	0.238	50	- 7.0	0.534
27 1/2	-20.5	0.251	54	- 4.75	0.604
29	-20.0	0.258	77	- 0.5	0.752
31	-19.5	0.266			

* Data on bulk density of these beds appear on p. 123.
** All surface deposits were ice unless otherwise noted.

Table XXXV

Experimental Data for Run 31

Description of Run:
Bed length - 5 in.
Rotameter reading - 30.6 ft^3./hr.
Room temperature - 89°F.
Barometric pressure - 29.37 in. Hg

Description of Regeneration:
Bath temperature - 140°F.
Pressure of air supply - 40 psig
$H_o = 1012 \times 10^{-6}$

Elapsed time-min.	Surface* temperature °F.	H/H_o	Elapsed time-min.	Surface temperature °F.	H/H_o
0	-23.5	0.212	53	-15.5	0.334
4	-23.5	0.212	60	-12.5	0.396
19	-23.0	0.218	68	- 9.0	0.477
34	-20.0	0.258	84	- 4.5	0.614
40	-19.0	0.272	100	- 2.5	0.684
44	-18.0	0.289			

Data on weight of bed for Run 31:

Wt. of dessicant + tare -	99.12 gms.
Wt. of tare -	51.22
Wt. of dessicant *	47.90 gms.

Table XXXVI

Experimental Data for Run 32

Description of Run:
Bed length - 4 in.
Rotameter reading - 30.3 ft^3./hr.
Room temperature - 88°F.
Barometric presure - 29.48 in. Hg

Description of Regeneration:
Bath temperature - 140°F.
Pressure of air supply - 40 psig.
$H_o = 1012 \times 10^{-6}$

Elapsed time-min.	Surface* temperature °F.	H/H_o	Elapsed time-min.	Surface temperature °F.	H/H_o
0	-24.5	0.200	42	-11.0	0.430
8	-24.0	0.206	55	- 7.0	0.534
20	-21.5	0.238	61	- 4.5	0.614
28	-19.0	0.272	75	- 4.5**	0.744
32 1/2	-16.0	0.324	85	- 2.5**	0.816

Data on weight of bed for Run 32:

Wt. of dessicant + tare -	85.11 gms.
Wt. of tare -	48.06
Wt. of dessicant -	37.05 gms.

* All surface deposits were ice unless otherwise noted.
** Water

Table XXXVII

Experimental Data for Run 33

Description of Run:
Bed length - 4 in.
Rotameter reading - 87.0 $ft.^3$/hr.
Room temperature - 92.5°F.
Barometric pressure - 29.42 in. Hg

Description of Regeneration:
Bath temperature - 170°F.
Pressure of air supply - 40 psig.
$H_o = 1012 \times 10^{-6}$

Elapsed time-min.	Surface* temperature °F.	H/H_o	Elapsed time-min.	Surface temperature °F.	H/H_o
0	-39.5	0.0802	11 1/2	-22.0	0.232
4 1/2	-39.0	0.0826	14 1/2	-14.0	0.364
7 1/2	-37.5	0.0906	19 1/2	- 6.0	0.565
8 1/2	-34.5	0.110	25	+ 0.5	0.795
9 1/2	-30.5	0.141			

Data on weight of bed for Run 33:

Wt. dessicant + tare -	85.23 gms.
Wt. of tare -	47.57
Wt. of dessicant -	37.66 gms.

Table XXXVIII

Experimental Data for Run 34

Description of Run:
Bed length - 3 in.
Rotameter reading - 30.2 $ft.^3$/hr.
Room temperature - 85°F.
Barometric pressure - 29.40 in. Hg

Description of Regeneration:
Bath temperature - 170°F.
Pressure of air supply - 40 psig.
$H_o = 1012 \times 10^{-6}$

Elapsed time-min.	Surface* temperature °F.	H/H_o	Elapsed time-min.	Surface temperature °F.	H/H_o
0	-44.0	0.0602	30	-35.0	0.106
12	-43.5	0.0624	33 1/2	-31.5	0.135
16	-43.0	0.0644	36 1/2	-28.0	0.162
23	-40.25	0.0768	41	-20.5	0.251
25 1/2	-38.5	0.0851	45	-15.5	0.334
27 1/2	-37.0	0.0930	49	-10.5	0.442

Data on weight of bed for Runs 28-30, 34:

Wt. of dessicant + tare -	56.51 gms.
Wt. of tare -	29.99
Wt. of dessicant -	26.52 gms.

* All surface deposits were ice unless otherwise noted.